8-2002

A study of aerocapture into Venus orbit for future exploratory missions

Anthony Scott Craig
University of Tennessee

To the Graduate Council:

I am submitting herewith a thesis written by Anthony Scott Craig entitled "A study of aerocapture into Venus orbit for future exploratory missions." I have examined the final electronic copy of this thesis for form and content and recommend that it be accepted in partial fulfillment of the requirements for the degree of Master of Science, with a major in Aerospace Engineering.

James Evans Lyne, Major Professor

We have read this thesis and recommend its acceptance:

Robert E. Bond, Joe Iannelli

Accepted for the Council:
Carolyn R. Hodges

Vice Provost and Dean of the Graduate School

(Original signatures are on file with official student records.)

To the Graduate Council:

I am submitting herewith a thesis written by Anthony Scott Craig entitled "A Study of Aerocapture into Venus Orbit for Future Exploratory Missions." I have examined the final paper copy of this thesis for form and content and recommend that it be accepted in partial fulfillment of the requirements for the degree of Master of Science, with a major in Aerospace Engineering.

Dr. James Evans Lyne, Major Professor

We have read this thesis
and recommend its acceptance:

Dr. Robert E. Bond

Dr. Joe Iannelli

Accepted for the Council:

Vice Provost and Dean of Graduate Studies

A Study of Aerocapture into Venus Orbit for Future Exploratory Missions

A Thesis
Presented for the
Masters of Science Degree
The University of Tennessee, Knoxville

Anthony Scott Craig
August 2002

Acknowledgements

First I would like to thank my major professor, Dr. Evans Lyne for his support and guidance while I endeavored to complete my masters after the departure of my original advisor. Also, I would like to thank Dr. Joe Ianelli and Dr. Robert Bond for being part of my graduate committee.

For his assistance in the oblate gravity model of Venus, I would like to thank Dr. Alexander Konopliv of NASA's Jet Propulsion Laboratory. I also express gratitude to Mike Tauber of NASA for supplying the heating relations used for the Venus atmosphere.

Abstract

The potential application of aerocapture for future unmanned exploratory missions to Venus has been examined to determine if it is a viable means of capture into Venus orbit. While many probes have already been sent to Venus, none of them used an aerocapture maneuver to insert into orbit. All of them depended on bulky rocket motors to slow the craft down sufficiently to allow capture. Aerocapture uses the atmosphere to reduce the velocity of the craft until it is captured into orbit.

An Apollo configuration vehicle similar in size to the Pioneer probes of the early 1980's is examined over an entry velocity range of 11 km/s to 14 km/s for the entry corridor, minimizing post aerocapture delta-V, and stagnation point heating. Also included is an examination of changes in ballistic coefficient, an alternate angle of attack, and atmospheric dispersions. Because Venus is similar in size to Earth, the target orbit for all cases was an altitude of 407 km. Deceleration constraints were added in the research, after the size of the entry corridor was found to be much larger than expected.

Final results showed that aerocapture would be a viable means of insertion into Venus orbit for robotic missions. The entry corridor was found to be approximately 1.65 degrees at 11 km/s decreasing to approximately 1.0 degrees at 14 km/s. Estimates of the stagnation point heating also showed that modern materials would be able to withstand the entry and protect the craft.

Table of Contents

List of Tables

List of Figures

List of Symbols and Abbreviations

S	Reference area (m^2)
AOA	Angle of attack (degrees)
Gammai	Initial entry angle (degrees)
L/D	Lift to drag ratio
C_D	Coefficient of drag
C_L	Coefficient of lift
NASA	National Aeronautics and Space Administration
POST	Program to Optimize Simulated Trajectories
ΔV	Velocity increment (m/s)
LEO	Low Earth Orbit
B^*	Ballistic coefficient (kg/m^2)
V_1	Free-stream velocity (m/s)
q_r	Radiative heating rate (W/cm^2)
ρ_1	Free-stream density (N/m^2)
r_n	Nose radius (meters)
h_w	Wall enthalpy (Joules)
h_T	Total Enthalpy (Joules)
A	Apoapse altitude (meters)
P	Periapse altitude (meters)
R	Radius of Venus (meters)
μ	Gravitational parameter (m^3/s^2)

T	Target orbit altitude (meters)
g	Gravitational acceleration (m/s^2)
I_{sp}	Specific Impulse (seconds)
m_0	Initial mass
m	Final mass

Chapter 1

Introduction

Section 1-1 Background and Past Missions

A large amount of study has gone into the use of aerocapture as a means to save weight in low earth orbit (LEO), concentrating on the manned and unmanned Mars missions planned for the near future [3-11]. However, relatively little research has been conducted in using aerocapture to send probes to other celestial bodies. While Venus has been investigated with a variety of probes both from the United States and former Soviet Union, technology is constantly advancing. This requires sending new probes every few years to places already explored to make use of the new technologies to learn more about Venus.

Plagued with problems in the beginning, the Soviet Union was the driving force in the early days of exploration to send spacecraft to Venus. Even with multiple failures from their Venera series of spacecraft, they persevered and started the exploration of the Earth's sister planet. The Veneras discovered one of the most inhospitable environments imaginable with an atmosphere 96% carbon dioxide and on the order of 3% nitrogen, with only a trace amount of water vapor and other gases and pressures great enough to crush some of the earlier spacecraft. For reference, the pressure on the surface of Venus is approximately 92 bars which is equivalent to being almost a kilometer below the surface of the ocean.

Pressured by the space race of the 1960's, the United States also began sending probes to Venus. Beginning with Mariner 2, and continuing through with the recent Magellan mission, the United States was not plagued with the failures of the early Soviet Venus missions. However, the greatest benefit of sending probes, was obtaining data that was not given out by the Soviet Union. The greatest of the early probes was the Pioneer Venus mission, which gave us most of our current knowledge of the Venusian atmosphere.

Pioneer Venus consisted of two spacecraft, an orbiter and a multiprobe bus. The multiprobe bus consisted of 3 small probes and one large probe that entered the atmosphere at widespread points. These probes and the bus itself are where the atmospheric data was obtained. The orbiter was used to determine the gravitational model and examine the upper atmosphere. However, it was not until Magellan that the gravitational models were increased to the accuracy used in this research.

Section 1-2 Aerocapture

The definition of an aerocapture maneuver is to use the atmosphere of a celestial body to reduce the velocity of a spacecraft in order to capture the craft into an elliptical orbit from a hyperbolic trajectory about said celestial body. This differs from the aerobraking that was used in the Magellan mission, in which the craft dipped into the atmosphere changing the elliptical orbit shape until the desired orbit was achieved. While aerobraking has been used successfully, aerocapture has not been used on a mission to this date.

A quick calculation shows that for an entry velocity of 11 km/s, 925 kg of liquid oxygen/liquid hydrogen or 2571 kg of monopropellant hydrazine are required to capture a 300 kg vehicle into low orbit about Venus, with other fuel mass requirements plotted in Figure 1-1. This shows the savings in mass possible through using the atmosphere to decelerate the vehicle into orbit. However, even with the fuel savings, the craft must be able to withstand the forces and heating of reentry.

While aerocapture may sound like the most ideal method to insert spacecraft into orbit, many problems could arise. Many factors must be examined to see if aerocapture is viable for a specific mission. First, the cost of manufacture and weight of the heat shield is compared against using a propulsive system that will accomplish the same goal. The heating rate and total heat load must be analyzed to ensure that materials are available to withstand the conditions. Also in some instances, aerocapture becomes impossible due to the deceleration limits. If the overshoot boundary surpasses the deceleration limit, then the entry corridor closes and an aerocapture is not possible.

For an aerocapture to be successful, the spacecraft must dissipate enough energy to reduce the planetocentric orbital period from infinity to a finite amount, without excessive heating or deceleration. Figure 1-2 [22] shows an example trajectory with the different phases labeled. The entry angles, measured relative to the tangent of the outermost edge of the atmosphere, define the entry corridor, as seen in Figure 1-3 [22]. The entry angle is designated as negative to indicate a trajectory entering the atmosphere. The smallest angle determined is called the overshoot boundary, because anything smaller and the spacecraft will overshoot the target orbit. The largest angle is called the undershoot boundary, for the exact opposite reasoning. Anything larger than the

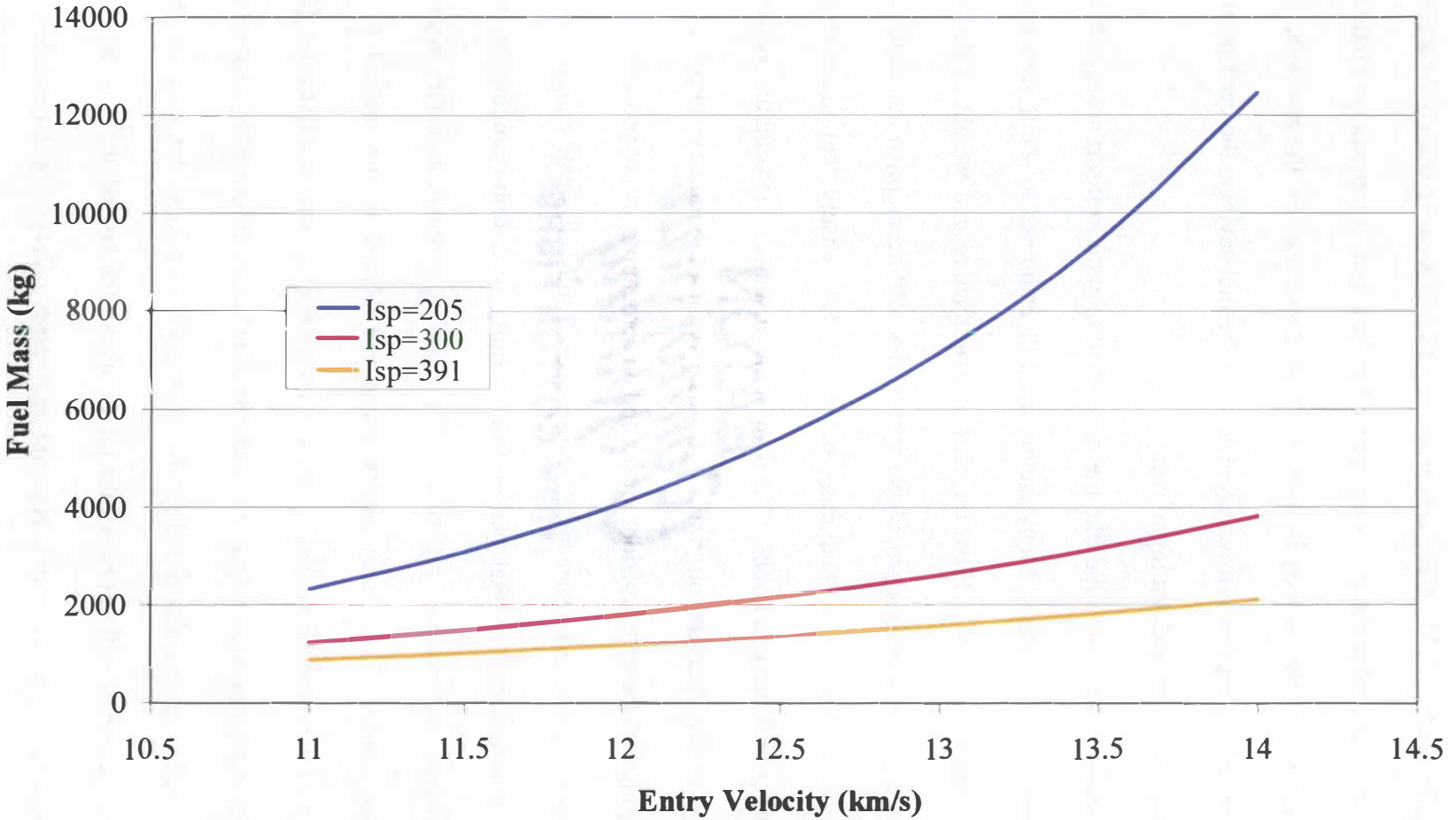

Figure 1-1: Fuel Mass Required to Insert a 300 kg Probe into a Circular Venus Orbit at 407 km

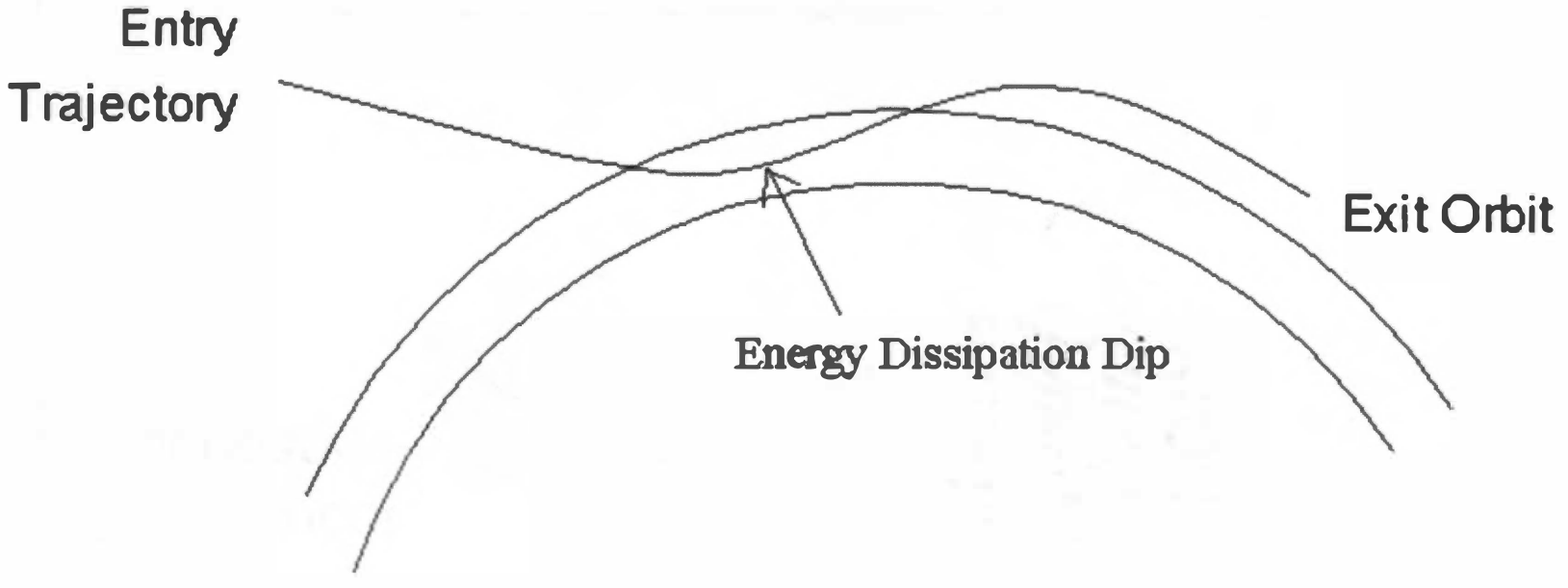

Figure 1-2: Aerocapture Maneuver Sequence

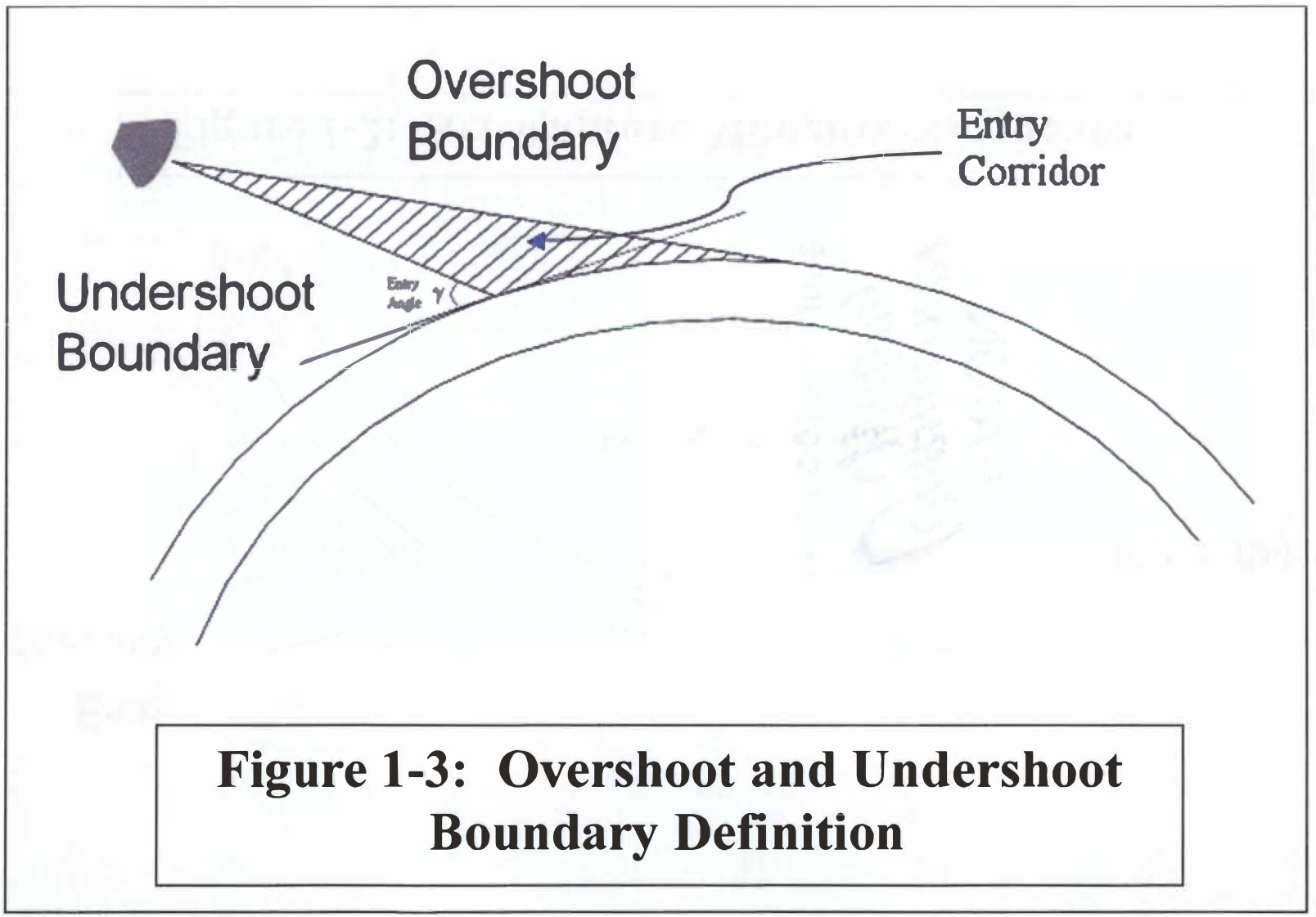

Figure 1-3: Overshoot and Undershoot Boundary Definition

undershoot boundary will undershoot the target orbit, causing the spacecraft to either crash on the planet surface, encounter excessive deceleration, or excessive heating. The entry corridor is dependent on many factors including, lift to drag ratio (L/D), ballistic coefficient, and entry velocity. Aerocapture studies for Mars has been examined in detail over the past few years, but it has not been methodically evaluated for Venus. It has been proven that a substantial amount of weight can be saved for the Mars missions. Even with the extreme conditions in the Venusian atmosphere, the preliminary results indicate that aerocapture can also be used to insert small spacecraft into Venus orbit.

Section 1-3 Objectives

This study follows the framework laid out by William D. Muth [3] and Cristoph Hoffman [4] in their master's thesis. It was attempted to use the same symbols and methodology whenever possible to start a set standard for these examinations. This paper will show the results of a preliminary study of aerocapture into Venus orbit for a modified Apollo configuration vehicle. The main objectives are as follows:

1) Determine the entry corridor over a range of entry velocities (11 km/s to 14 km/s) for nominal conditions as reported by the Pioneer Venus probes.
2) Determine the effects on the entry corridor for the off-nominal atmosphere, alternate ballistic coefficient, and alternate aerodynamic coefficients.
3) Determine the velocity increment, ΔV, required to circularize the orbit following aerocapture with a period of approximately ninety minutes.

4) Perform initial studies on stagnation-point heating rates and total integrated heat load for both radiative and convective heating.

Chapter 2

Vehicle Specifications

The vehicle used for the analysis was a modified Apollo capsule. The Apollo capsule was chosen due to the large amount of data acquired from the Apollo program. The modified capsule was the same shape as the original Apollo capsule, but scaled down to the approximate size of the Pioneer Venus large probe. The nominal vehicle had a radius of 1 meter, a mass of 300 kilograms, a lift to drag ratio (L/D) of 0.35 and an effective nose radius of 1.92 meters. In comparison, the Pioneer Venus large probe had a radius of 0.75 meters and mass of 315 kilograms [21], but was used for a ballistic entry, i.e. lift was not produced.

One difficulty in using the Apollo vehicle was the aerodynamic data was only given for a set angle-of-attack (AOA). To overcome this, a NASA website called IDS was intended to be used [17]. Unfortunately, the IDS website no longer works, but the aerodynamic coefficients for the Apollo capsule were calculated using IDS several years ago by a senior design team at the University of Tennessee [22]. Table 2-1 shows the accuracy of the IDS analysis when compared to the actual Apollo data taken at an AOA

Table 2-1: Percent Error of IDS Curve Fit when Compared to Actual Apollo Values at an AOA of 156.7 degrees

	Actual Value	IDS Curve Fit Value	Percent Error
Drag Coefficient	1.224	1.107	9.58
Lift Coefficient	0.4321	0.400	7.53

of 156.7 degrees. The IDS data is output in tabular form and a curve fit was made, as seen in Figure 2-1, to determine values of the coefficients at a given AOA. Figure 2-2 shows the convention used to define the AOA. The curve fits were then used to determine the AOA at which the Apollo craft has an L/D of approximately 0.20. The alternate AOA was used to show how the entry corridor changes with different aerodynamic coefficients. The 10 percent error in the IDS data was not deemed excessive because this was a preliminary analysis.

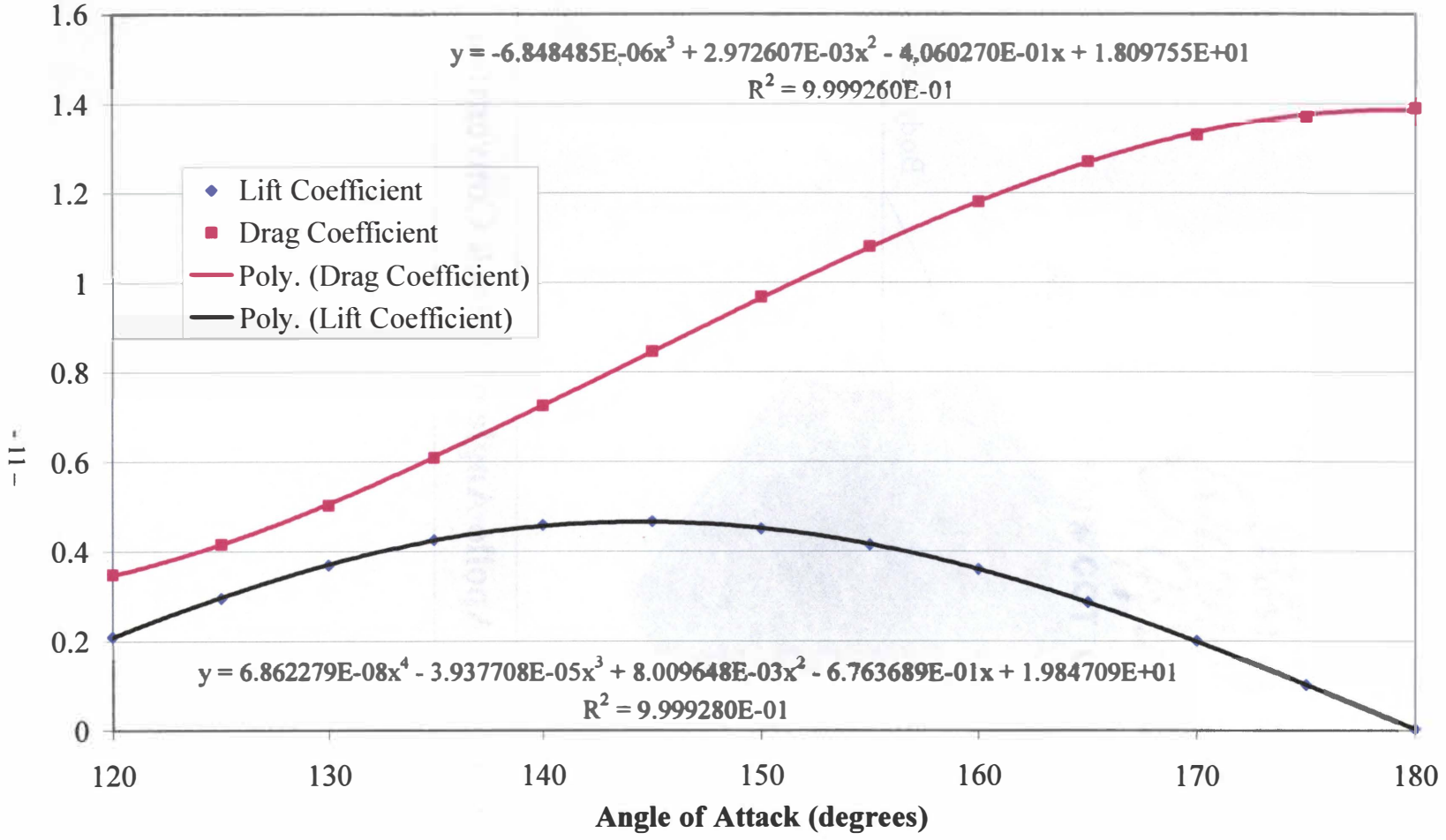

Figure 2-1: Estimated Apollo Aerodynamic Coefficients Using IDS

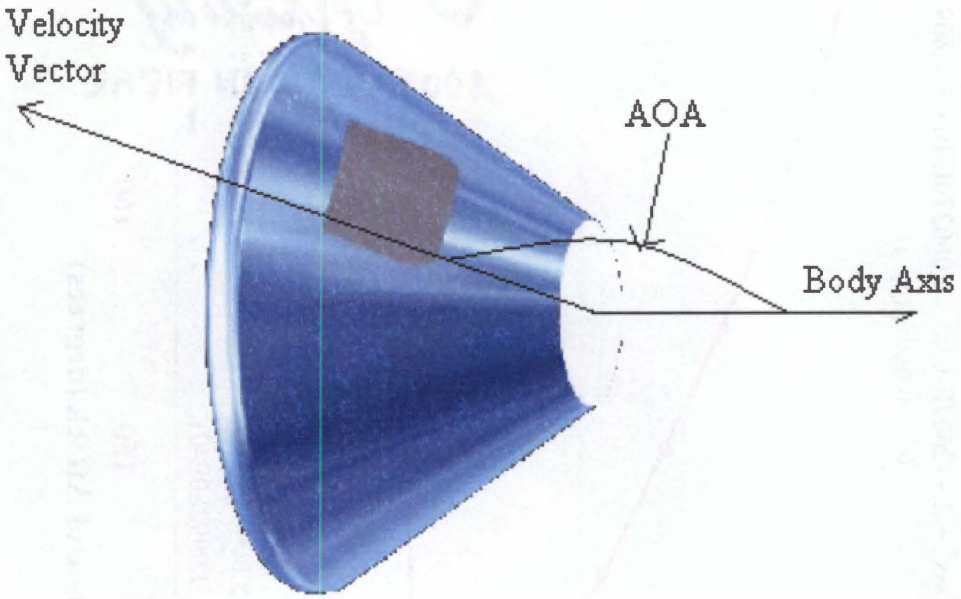

Figure 2-2: Apollo Angle of Attack Convention

Chapter 3

Methodology

Section 3-1 Program to Optimize Simulated Trajectories

NASA's Program to Optimize Simulated Trajectories (POST) was first developed for use with the Space Shuttle in 1970 [14]. Since then it has undergone many revisions and upgrades to make it capable of analyzing trajectories for a number of different mission parameters, as seen in Table 3-1. Written in FORTRAN for a UNIX based environment, POST consists of an input deck, program files and various output files. The input deck controls all the user-specified parameters including aerodynamics, atmospheric conditions, integration method, and many others.

For the analysis, the three-degree of freedom (3-D) version of POST was used. While there is a six-degree of freedom version, the rotational components were neglected in this initial study, leaving only the translational components of the 3-D version. POST models the craft as a point mass and gives the capability to target and optimize for a given set of end conditions. This includes both powered and unpowered craft in the sphere of influence of a single arbitrary celestial body. While POST is defaulted to Earth conditions, all parameters can be changed to fit with any other celestial body, provided the data is available.

In order to start working with POST, an input deck must first be constructed. The input deck gives the user-specified criterion that must be met to solve the problem, along with any independent variables that affect the final answer. The first parameters set in

Table 3-1: Typical Applications of POST [23]

Type of Mission	Type of Vehicle	Optimization Variable	Typical Constraints	
			Equality	Inequality
Ascent to Near-Earth Orbit (2 - 20 min cpu time)	Titan, Space Shuttle, Single Stage to Orbit (VTO and HTO)	Payload, Weight at Burnout, Propellant, Burntime, Ideal Velocity	Radius, Flight Path Angle, Velocity	Dynamic Pressure, Accelerations
Ascent to GeoSynch Orbit (3 - 50 min cpu time	Titan, Space Shuttle/Upper Stage	Payload, Propellant	Apogee, Perigee, Inclination	Dynamic Pressure, Angle of Attack, Pitch Rates
Ascent Abort (2 - 5 min cpu time)	Space Shuttle	Abort Interval	Landing Site Latitude and Longitude	Dynamic Pressure, Acceleration
ICBM Ballistic Trajectory (2 - 20 min cpu time)	Titan, Minuteman, Peacekeeper	Payload, Miss Distance	Latitude, Longitude, Downrange, Crossrange	Reentry Flight Path Angle, Acceleration
Reentry (3 - 15 min cpu time)	Space Shuttle, X-24C, Single Stage to Orbit	Heat Rate, Total Heat, Crossrange	Latitude, Longitude, Downrange, Crossrange	Heat Rate, Acceleration
ICBM Orbital Maneuvers (0.5 - 10 min cpu time)	Titan, Transtage, Centaur,IUS, Solar-Electric Propulsion	Payload, Propellant, Ideal Velocity, Burntime	Latitude, Semimajor Axis, Eccentricity, Inclination, Argument of Perigee, Period	Reentry Attitude Angles, Perigee Altitude
Aircraft Performance (0.1 - 5 min cpu time)	X-24B and C, Subsonic Jet Cruise, Hypersonic Aircraft	Mach, Cruise Time, Payload	Downrange, Crossrange, Dynamic Pressure, Mach, Altitude	Dynamic Pressure, Max Altitude Dynamic Pressure

the input deck are the integration and targeting method and the unit's flags. Then, the dependant and control variables are defined and assigned a target and intial value respectively. The dependant variables are measured and control variables occur at a given phase. A number defines the phase and POST can accommodate an unlimited number of phases. While perturbation sizes are set at a default in POST, they can be changed in case the default perturbation does not allow for convergence to an optimized trajectory.

In order to model another planet, several different parameters must be changed from the defaults. First, the atmospheric data stored in POST are all Earth based models, and if another planet is to be modeled, then a density profile must be defined. The density profile can either be defined as a function versus altitude or input in tabular form. The density tables used were from the Pioneer Venus missions [2] and are shown as a logarithmic plot in Figure 3-1. Next, all planets are not perfectly spheroid, so the oblate planetary model should be used for more accurate results. The recent Magellan mission has produced the most accurate oblate gravitational model for Venus to date [1]. For this analysis, only the first eight constants were used. Finally, the gravitational parameter (μ), rotational period, and polar and equatorial radii must be obtained.

Once the planet has been defined, the spacecraft parameters need to be set. Although POST is a very powerful tool for determining trajectories, it cannot determine the aerodynamic coefficients of a vehicle. These must be obtained from an external source. For the nominal Apollo configuration, the actual coefficients from the Apollo program [13] were used. To determine the alternate AOA used later in the analysis, NASA's IDS website was used as stated in the previous chapter. The reference area and mass are also required for input. The nose radius can be input if POST is to do the

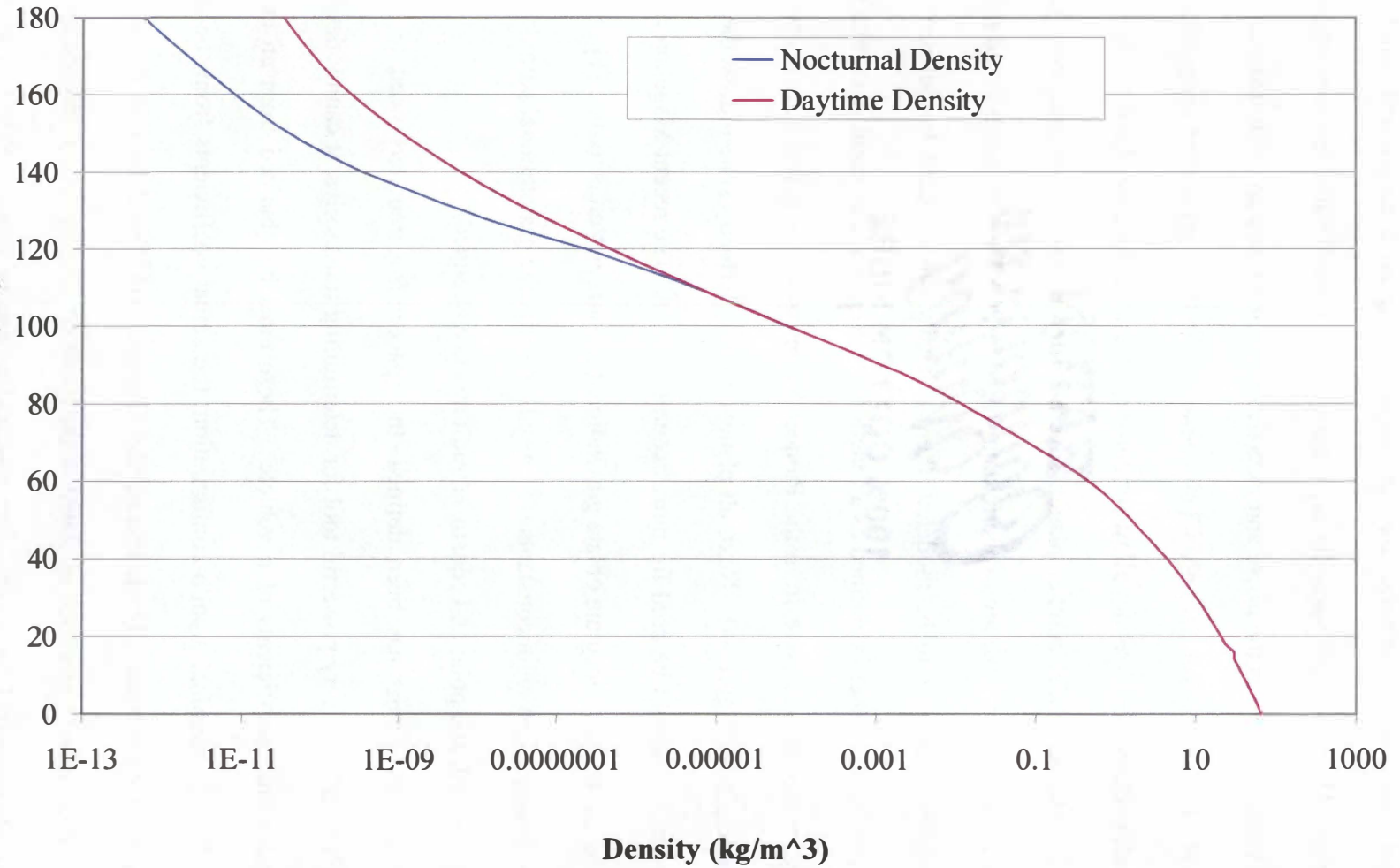

Figure 3-1: Density Profiles for Venus

heating calculations, but another method was used for this analysis. In the last step, the phases are defined, including the final phase that ends the problem.

Section 3-2 Aerocapture Simulations

Aerocapture simulations in POST require some specific parameters to be defined. For all the simulations run, a fourth order Runge-Kutta integration with a time step of one second was used. Then came the entry velocity, this is the velocity at which the spacecraft first enters the simulation. Next, the initial entry angle, gammai, was input, but only as an initial guess, as POST was set up to optimize for gammai for all runs. Also, the vehicle entered the atmosphere at 0 degrees longitude and 0 degrees geocentric latitude.

The atmosphere of Venus posed a unique problem to aerocapture. The extremely high densities in the lower atmosphere meant that the altitude must be monitored carefully to prevent excessive heating. Below 100 kilometers, Venus's atmosphere increases in density dramatically, but above 100 kilometers, the atmosphere dissipates just as dramatically. The upper limit of the atmospheric data was 180 kilometers, so all POST runs began at this point. Atmospheric winds were neglected, because the winds are very small in magnitude above roughly 90 kilometers [2]. However, if a trajectory dropped to the first cloud layer, winds could not be neglected as they were clocked at approximately 100 meter/second by the Venera probes at the top of the clouds, or 70 km in altitude [15]. All POST runs were also completed using the nocturnal atmosphere unless otherwise specified.

The only constraint held throughout all the runs was a target apoapse of approximately 407 kilometers. The orbit, after circularization, would give an orbital period of about 95 minutes. This period and altitude is similar to the many satellites currently orbiting Earth in low orbit. For an overshoot trajectory, the vehicle enters at a bank angle of 180 degrees so the lift vector is directed toward the surface. For an undershoot trajectory, the vehicle initially enters with the lift vector pointing away from the planet or a bank angle of zero degrees. Then several different procedures were analyzed. First, the bank angle was held at zero degrees to obtain the maximum corridor possible for the vehicle at a given speed. Then, the periapse was targeted at 112 km or 107 km, depending on the aerodynamics. Finally, a deceleration limit was imposed at 20 G, where 1 G is the acceleration felt on the surface of Earth. The roll rates for all bank angle modulations were set at a constant 10 degrees/sec.

Chapter 4

Analysis and Results of the Nominal Vehicle (L/D = 0.35)

Section 4-1 Entry Corridor

As stated earlier, the entry corridor is the difference between the undershoot and overshoot angles. These angles are dependent on a number of different parameters that will each be discussed in turn. The entry corridor is all-important when it comes to atmospheric entries. Because the corridors are typically small, on the order of a degree or less, they must be calculated as accurately as possible to allow for any errors that may come about in flight. It should also be noted that the vehicle is very unlikely to enter exactly at the undershoot or overshoot boundary. These are calculated as the limits of the corridor, and in the case of the undershoot, gives the most severe conditions the spacecraft will face in the trajectory.

Section 4-1.1 Undershoot Boundary

The undershoot boundary of an entry trajectory are the defining factors in determining the peak heating and deceleration for the vehicle. Initially, the undershoot boundary was calculated without using roll maneuvers. This gives the absolute maximum angle that the vehicle can enter the atmosphere and still be able to reach the target apoapse. When this analysis was performed it was found that, the periapse was below the surface of the planet for all runs. While this can be corrected with an orbital burn, the purpose of aerocapture is to save mass by minimizing fuel consumption. As

seen in Table 4-1, the periapse becomes smaller as entry velocity increases. The extremely low periapse is attributed to the high entry angle required for these trajectories. Because the vehicle is entering with the lift vector pointing away from the planet at all times, the entry angle must be higher considerably steeper than the overshoot angles. Otherwise, the vehicle would not dissipate sufficient energy to capture into the prescribed orbit. If the periapse was targeted, then the entry angle would be less, but the apoapse would increase dramatically. Figure 4-1 shows the altitude and deceleration history for an undershoot boundary trajectory with no roll maneuvers at an entry velocity of 12 km/s.

Section 4-1.2 Overshoot Boundary

The overshoot boundary is the minimum angle the vehicle can enter the entry trajectory and still reach the target orbit. Found by maintaining the lift vector pointing towards the planet at all times, it proved to be much more difficult to compute than the undershoot. POST can calculate the overshoot boundary in one of two ways. First, the entry angle can be modified manually for every run until the trajectory meets the target orbit. Second, POST can optimize the entry angle until the target orbit is reached. Although the second method sounds easier, it proved not to be the case. Due to the high accuracy needed for the overshoot, POST would typically run up to 20 minutes, but still not give the correct angle. The angle output would need to be reentered in POST and run again until it converged on the solution. In the end, both methods proved to be as time consuming, with the second method used predominately throughout the analysis.

The overshoot trajectory also gives the most benign trajectory the vehicle can follow in terms of deceleration loads and peak heating rates, but experiences much higher

Table 4-1: Undershoot Boundary (no roll maneuvers)

Velocity (km/s)	Entry Angle (deg)	Apoapse Altitude(km)	Periapse Altitude (km)	Peak Deceleration (G)
11	-8.499437126	413.05	-651.74	22.29
11.5	-8.99272495	414.53	-791.48	28.98
12	-9.459862942	412.01	-944.01	36.78
12.5	-9.896449563	416.23	-1075.10	44.82
13	-10.32285357	413.10	-1229.70	53.42
13.5	-10.72036942	416.69	-1355.50	64.74
14	-11.1175564	412.20	-1513.00	75.85

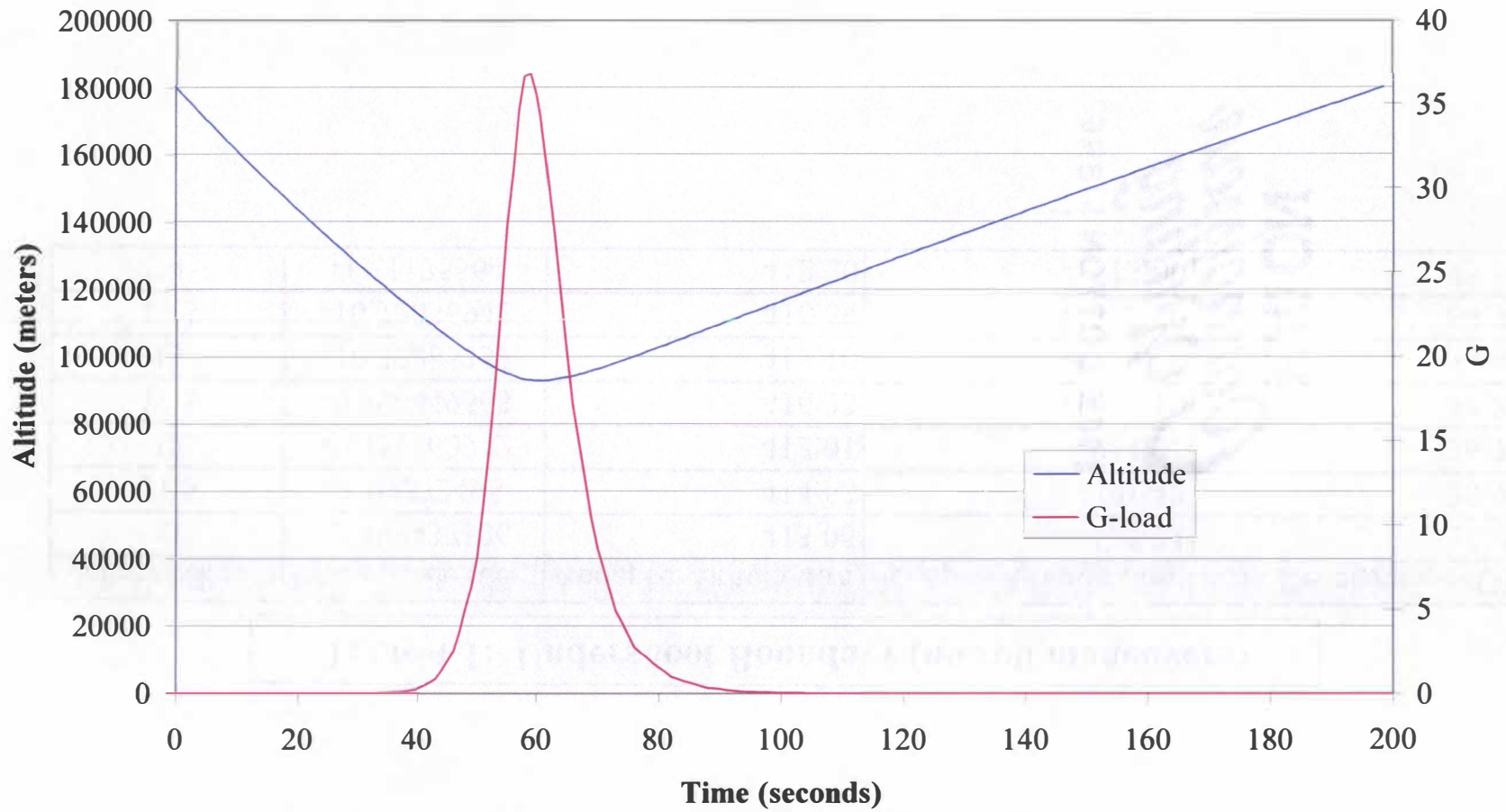

Figure 4-1: Undershoot Boundary (no roll maneuvers) Altitude and Deceleration History for 12km/s for the Nominal Vehicle (L/D=0.35)

total heat loads. As seen in Table 4-2 and compared to Table 4-1, the decelerations encountered by the vehicle are significantly less than the undershoot. It should also be noted that the periapse of all the overshoot trajectories are approximately equal. The altitude history on Figure 4-2 shows that the vehicle exits the atmosphere much more gradually than the undershoot case. This raises the periapse and because all the overshoot trajectories exit the atmosphere at a similar angle, they're periapses are nearly equal.

Section 4-1.3 Entry Corridor

The difference between the undershoot and overshoot boundaries define the entry corridor. The entry corridor represented by these two boundaries represent the maximum possible corridor for that given entry speed with the given aerodynamics, neglecting changes in the atmosphere. Figure 4-3 shows the surprising result that the entry corridor actually increases as the entry velocity increases from 11 km/s to 14 km/s. The increase in the entry corridor was created by a lack of targeting the periapse or constraining deceleration. The past aerocapture studies were completed for manned missions where deceleration must be constrained otherwise the crew would not survive the reentry. Unmanned probes are not as affected by this, sometimes withstanding several 100's of G's compared to the 5 G limit imposed on the Mars Mission studies. However, the deceleration for larger entry velocities could be excessive, so a reasonable deceleration limit was examined after targeting the periapse.

Table 4-2: Overshoot Boundary

Velocity (km/s)	Entry Angle (deg)	Apoapse Altitude (km)	Periapse Altitude (km)	Peak Deceleration (G)
11	-6.63365084	411.04	113.61	2.04
11.5	-6.855300309	412.73	113.60	2.52
12	-7.044587716	412.06	113.60	2.94
12.5	-7.207920356	415.54	113.59	3.36
13	-7.350113644	412.65	113.60	3.8
13.5	-7.474837739	410.85	113.61	4.25
14	-7.584963239	411.62	113.60	4.72

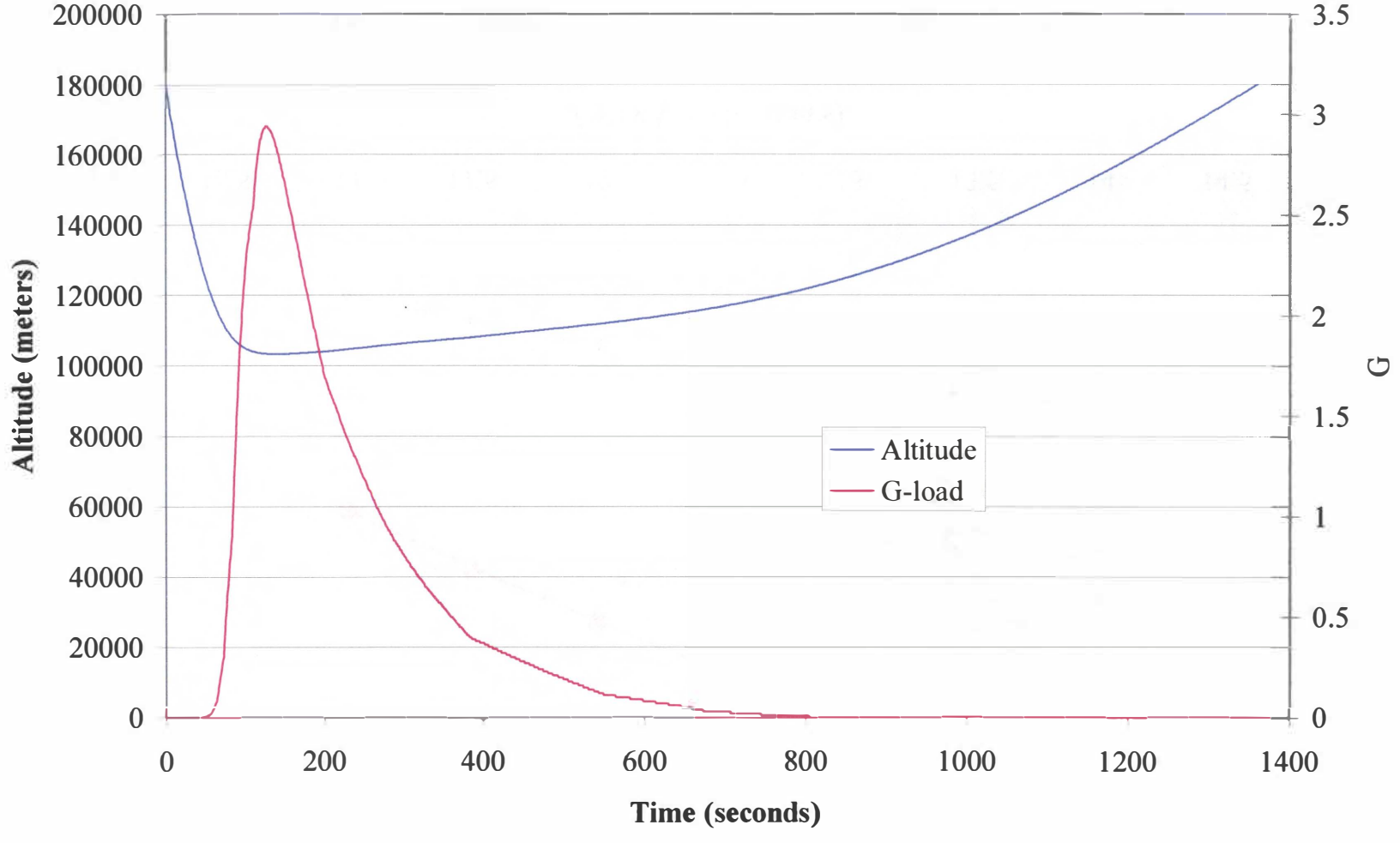

Figure 4-2: Overshoot Boundary Altitude and Deceleration History for 12km/s for the Nominal Vehicle (L/D=0.35)

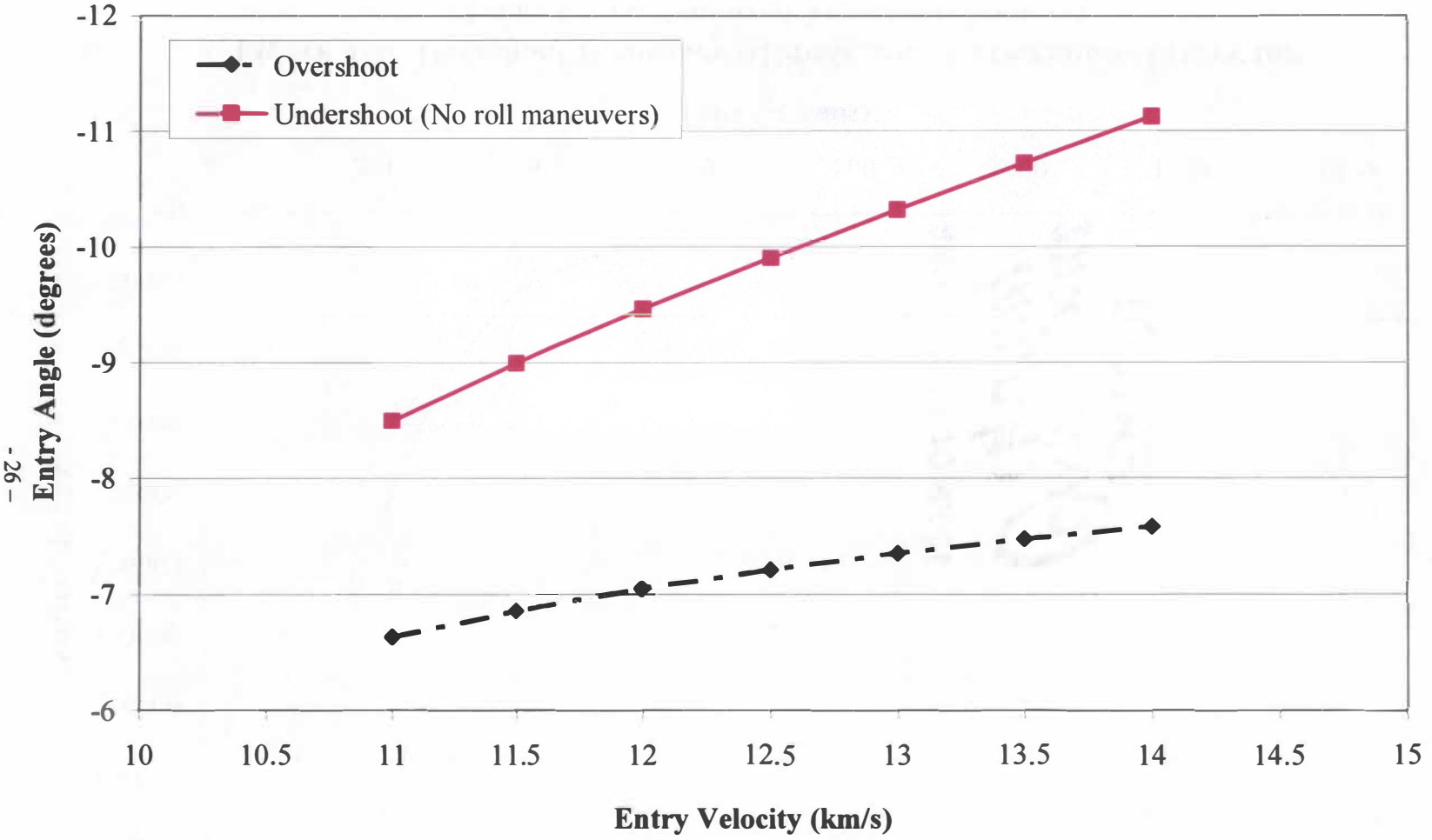

Figure 4-3: Nominal Vehicle Maximum Entry Corridor

Section 4-2 Bank Angle Modulation

After the initial entry corridor was calculated, it became evident that the undershoot boundary was too high for an optimal trajectory due to the extremely low periapse. Although the undershoot does reach the target apoapse altitude, the periapse was extremely low when compared to the overshoot. Thus, some aerodynamic maneuvers had to be performed while still in the atmosphere in order to raise the periapse. By modulating the bank angle, the lift vector is changed from pointing away from the planet to pointing toward the planet. This accomplishes two things. First, more energy is dissipated so the entry angle must be reduced, and second, it raises the periapse considerably from the original undershoot. Two different targets were selected to analyze how the undershoot changes.

Section 4-2.1 Targeted Periapse

First, the periapse was given a target value of 112 km with a tolerance of 10 km. This was chosen from the overshoot boundary which gave a periapse of approximately 113 km, and the undershoot boundary's periapse were smaller than the overshoot boundary. Then a roll maneuver of 180 degrees at 10 deg/sec was added with POST calculating the best time to start the roll. With the new constraint and control, POST was again run for the same entry velocities. The resulting undershoot boundary was considerably more benign than the untargeted periapse trajectories, as was expected. Table 4-3 shows the apoapse, periapse and peak deceleration for the targeted periapse case. POST had some difficulty targeting both the apoapse and periapse at the higher entry velocities and the best values were recorded for both 13.5 and 14 km/s entry speeds.

Table 4-3: Undershoot Boundary (targeted periapse)

Velocity (km/s)	Entry Angle (deg)	Apoapse (km)	Periapse (km)	Peak Deceleration (G)	Time to Roll Maneuver (sec)
11	-7.91246286	407.43	104.38	14.21	85.6869044
11.5	-8.20631742	414.98	109.86	16.89	78.2298516
12	-8.54200000	416.03	109.91	21.62	70.8842000
12.5	-8.88175970	419.73	108.58	26.95	64.4195931
13	-9.22495162	410.71	108.19	32.62	58.7912932
13.5	-9.49084899	383.26	105.19	39.08	54.3025560
14	-9.75905424	379.71	103.49	46.51	50.2305210

Figure 4-4 shows the deceleration and altitude history of a 12 km/s entry speed with targeted periapse. Looking at the chart, the roll maneuver can be seen at approximately 71 seconds into the trajectory as a change in inflection in the curve.

Section 4-2.2 Deceleration Constraint

An evaluation of constraining the deceleration of the vehicle was examined due to some of the higher G-loads experienced by the vehicle at large entry velocities. A limit of 20 G was imposed to preserve components contained within the spacecraft. This limit was taken from data on the highly successful Mars Pathfinder mission [23] and seemed to be a reasonable limit when compared to some of the G-loads experienced from the unconstrained cases. Referring back to Table 4-3, the lower entry velocities already met this criterion while targeting the periapse, so it was expected that gammai for these velocities would be larger than the targeted periapse case. It should be noted that the periapse was not targeted for the deceleration constraint study. However as seen in Table 4-4, the periapse for entry speeds of 12 km/s and above still reached the target periapse. This is due to the nature of the trajectory and the roll times involved. Figure 4-5 shows the altitude and deceleration history at 12 km/s for this case. Calculated by POST, the time to the roll maneuver for the deceleration constraint was slightly longer at about 72 seconds.

Section 4-2.3 Modified Entry Corridor

Applying the new constraints changes the width of the entry corridor. Although the corridor shrinks, the added constraints give a better estimate of the corridor used for a

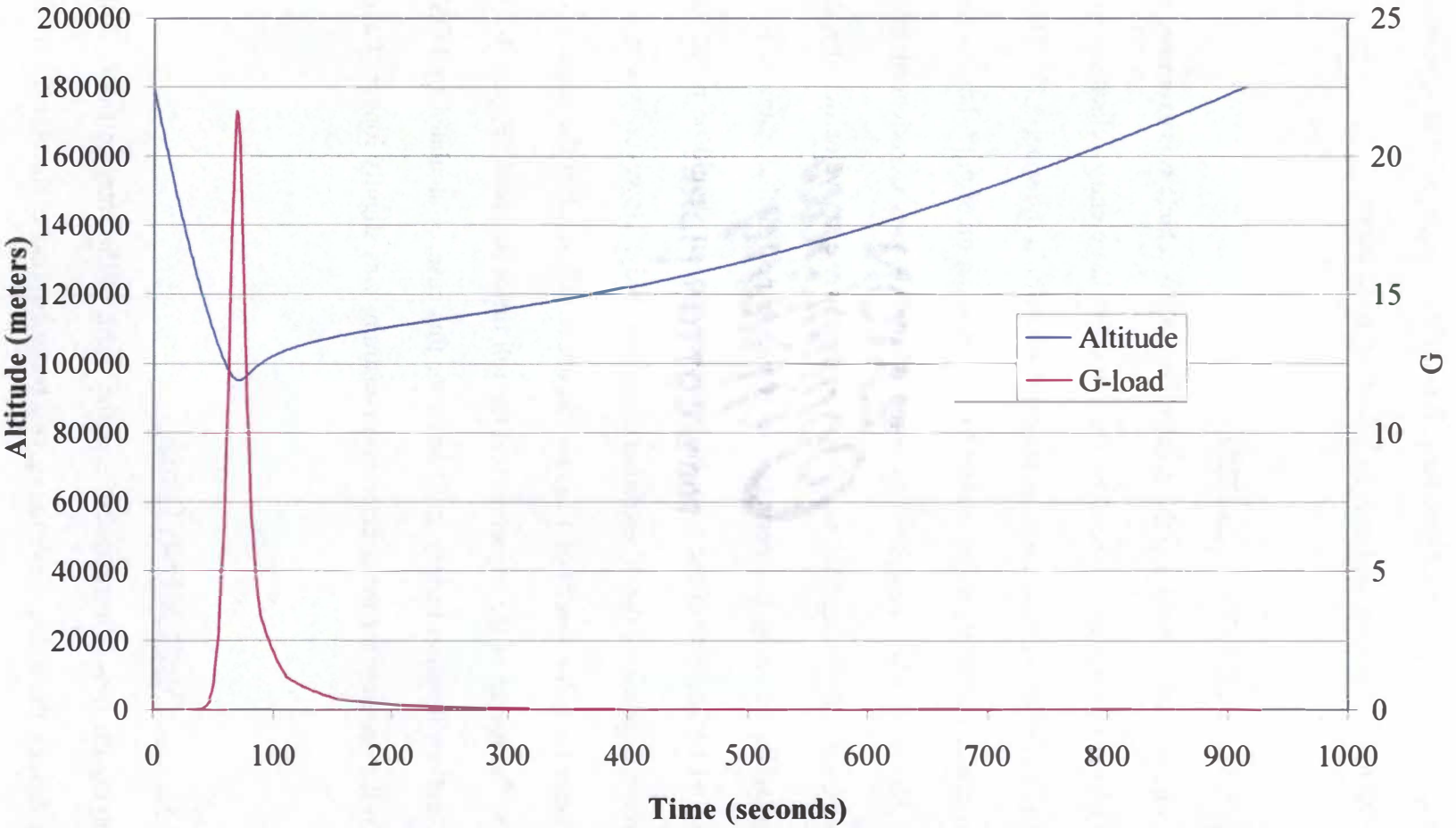

Figure 4-4: Undershoot Boundary (targeted periapse) Altitude and Deceleration History for 12km/s for the Nominal Vehicle (L/D = 0.35)

Table 4-4: Undershoot Boundary(deceleration constraint)

Velocity (km/s)	Entry Angle (deg)	Apoapse (km)	Periapse (km)	Peak Deceleration (G)	Time to Roll Maneuver (sec)
11	-8.307584645	407.92	-152.55	19.99	82.67954784
11.5	-8.380676227	404.48	90.34	20	75.80479415
12	-8.459496173	406.40	112.02	19.99	71.98798239
12.5	-8.530601877	403.96	113.39	20	68.66085015
13	-8.578406303	414.15	113.53	20	65.72687364
13.5	-8.607028557	405.83	113.58	20	63.12411715
14	-8.636009675	407.14	113.58	20	60.67771082

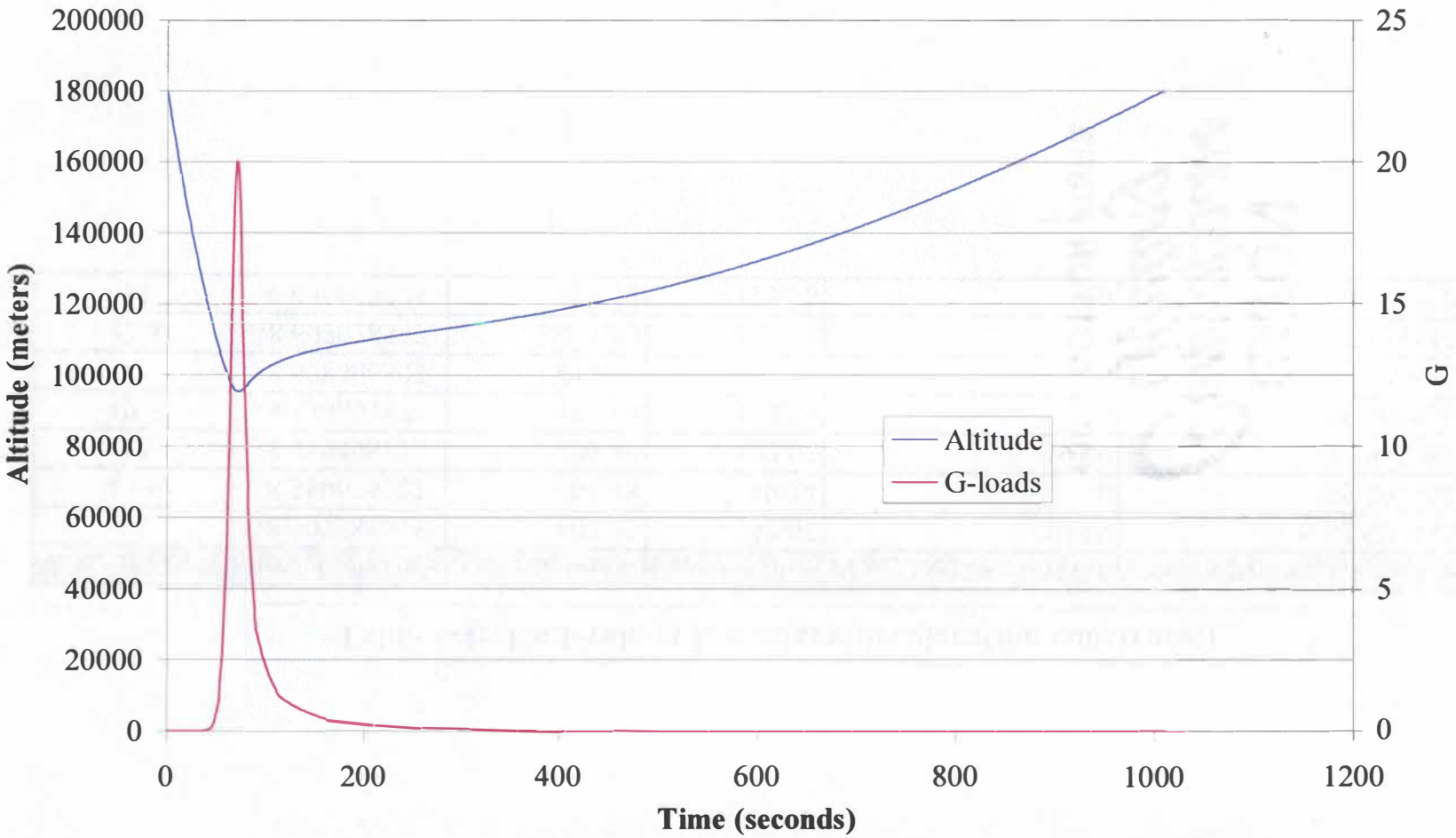

Figure 4-5: Undershoot Boundary (deceleration constraint) Altitude and Deceleration History for 12km/s for the Nominal Vehicle (L/D=0.35)

realistic mission. The low periapse of the undershoot boundary with no roll maneuvers would require a much larger velocity increment to correct when compared to the targeted periapse or even the deceleration constraint. Figure 4-6 shows the overshoot and all three undershoot boundaries for comparison.

As seen in Figure 4-6, the corridor is on the order of one degree or more in width depending on which constraint is in place. However, if both the deceleration is constrained and periapse is targeted, then the boundary would be the overshoot and the next higher point. For example, at 11.5 km/s, the corridor would be the overshoot and the undershoot with the targeted periapse, but at 13 km/s the corridor would be the overshoot and the undershoot with the constrained deceleration.

Section 4-3 Atmospheric Dispersions

The analysis up to this point centered on a constant atmosphere, i.e. no temperature changes due to weather. While it has been shown that the Venusian atmosphere is nearly constant at the surface, the upper atmosphere can vary greatly from day to night. Also, the temperature can vary up to 10 Kelvin at the lower altitudes in the trajectory. The temperature change also can change the density of the atmosphere which requires analysis to confirm that the entry corridor remains open for an off-nominal day.

Section 4-3.1 Diurnal Atmospheric Changes

Venus rotates about its axis once every 243 Earth days. This provides that atmosphere ample time to absorb or disperse a considerable amount of energy from the sun on the day or night side respectively. Below 100 kilometers in altitude, the

atmosphere is essentially constant diurnally. However above this, the temperature starts to change at 100 kilometers until at 180 kilometers, the limit of the atmospheric data, the temperature is 300 K during the day, but only 170 K at night. Initially, this would seem to change the entry corridor, but as seen in Figure 4-7, it is virtually unchanged at less than 1% of the nocturnal values. Looking at the atmospheric data, the densities in the upper atmosphere are sufficiently low that there is very little aerodynamic effect.

Section 4-3.2 Dispersion Modeling

Temperature changes in the atmosphere can affect the free stream density encountered by the entry vehicle. This can affect the width of the entry corridor, or in the case of unconstrained deceleration, cause higher G-loads on the spacecraft. Given that the temperature at 100 kilometers can change as much as 10 Kelvin, a 30% variation in density data was applied to the atmospheric tables. POST has a function that allows the user to apply a multiplier to a table so the entire table need not be reentered. The density table was then multiplied by 0.7 and 1.3 for the uncertainty. Typically, the overshoot is affected by the low density case, and the undershoot is affected by the high density case. Figures 4-8 through 4-11 show the various boundaries compared with their off-nominal cases and Figure 4-12 shows the entry corridor with the most confining conditions.

Figures 4-8 and 4-9 both show what is expected of an off-nominal calculation. All three lines are similar, but are offset from each other slightly. Figures 4-10 and 4-11, however, show more variation in the boundaries. Figure 4-10 is the targeted periapse, which POST had some difficulty in targeting the higher entry velocities. The targeted apoapses for entry speeds of 13.5 and 14 km/s on the nominal atmosphere were outside of

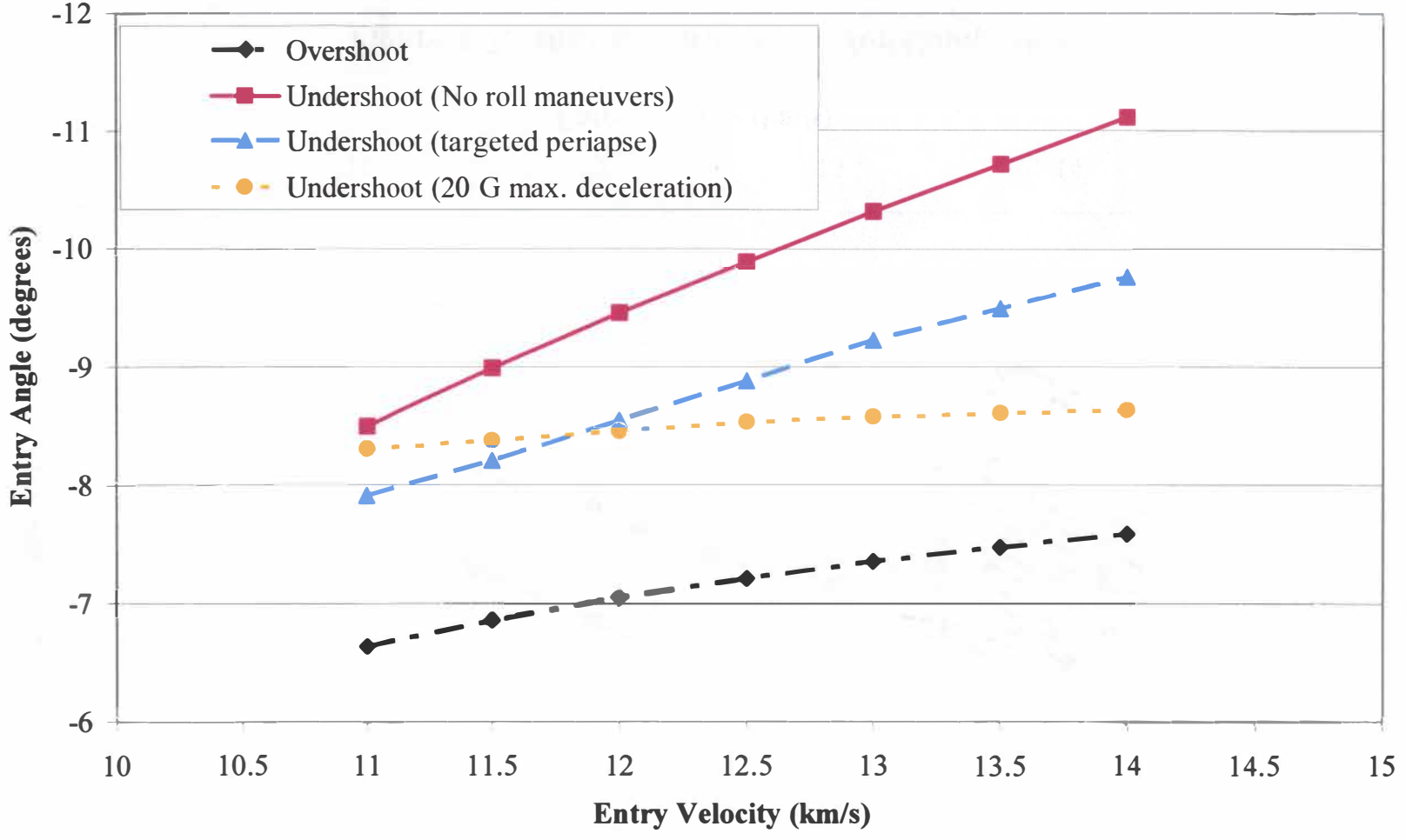

Figure 4-6: Modified Entry Corridor

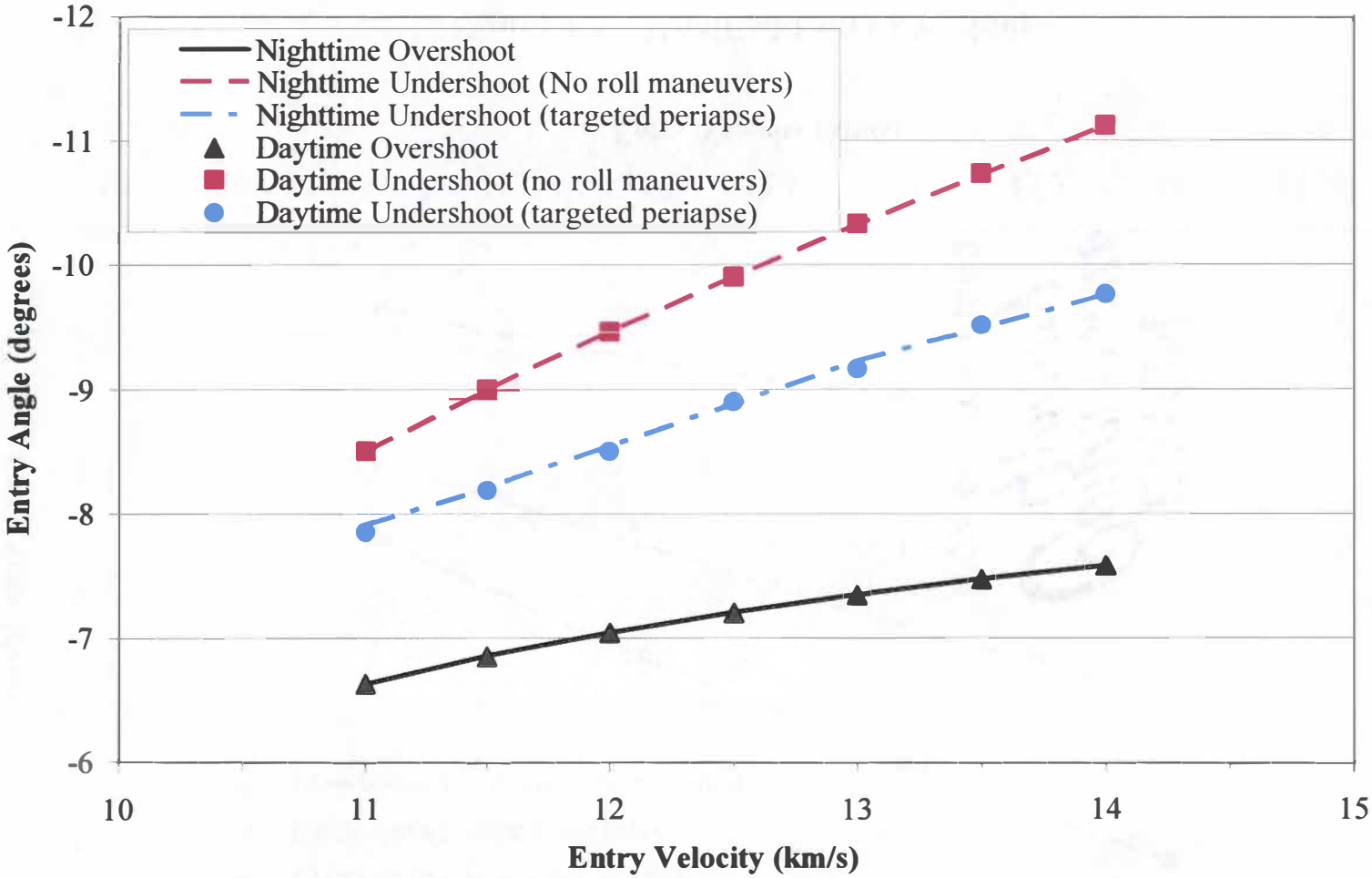

Figure 4-7: Diurnal Entry Corridor Comparison

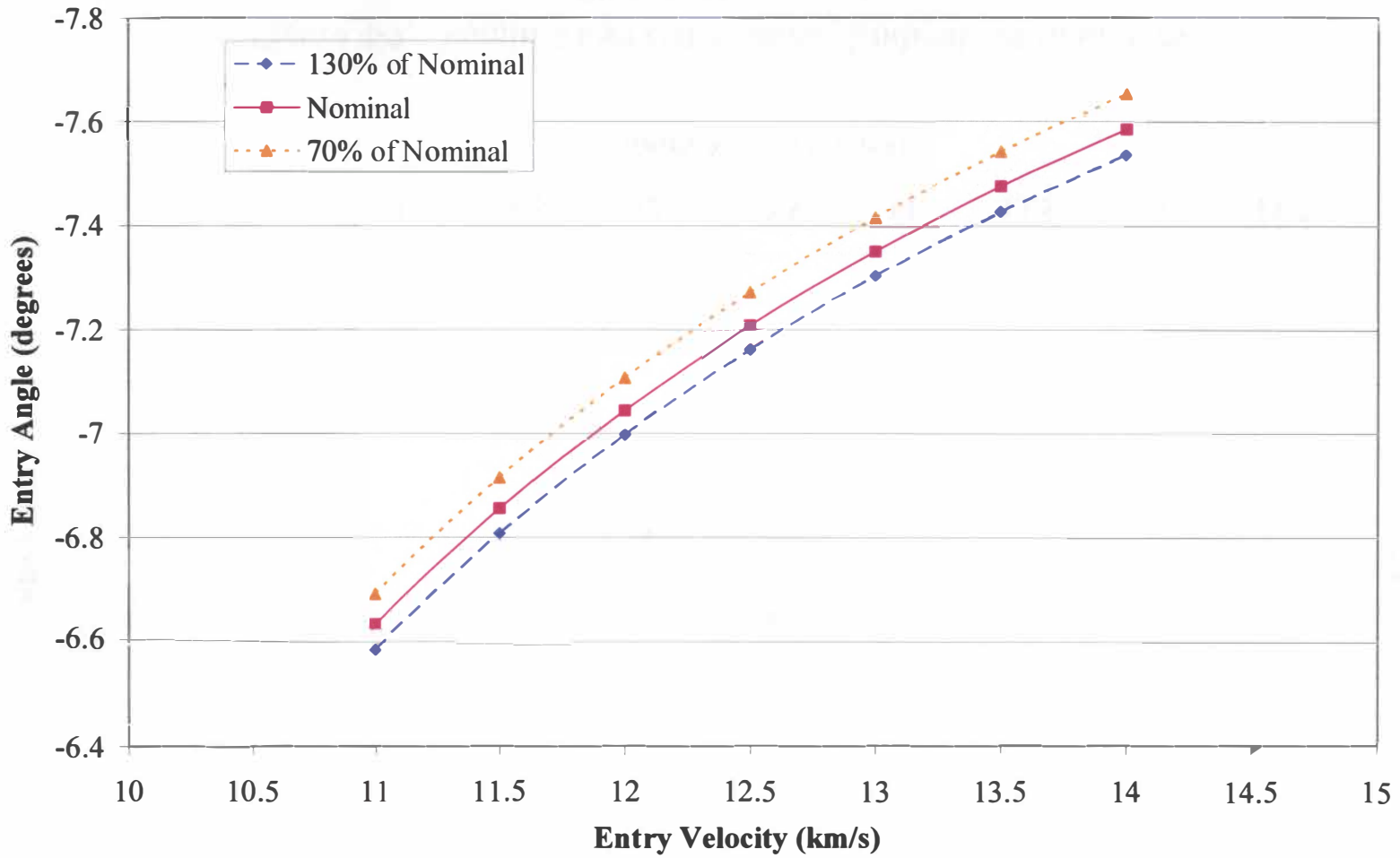

Figure 4-8: Nominal and Off-nominal Overshoot Boundary

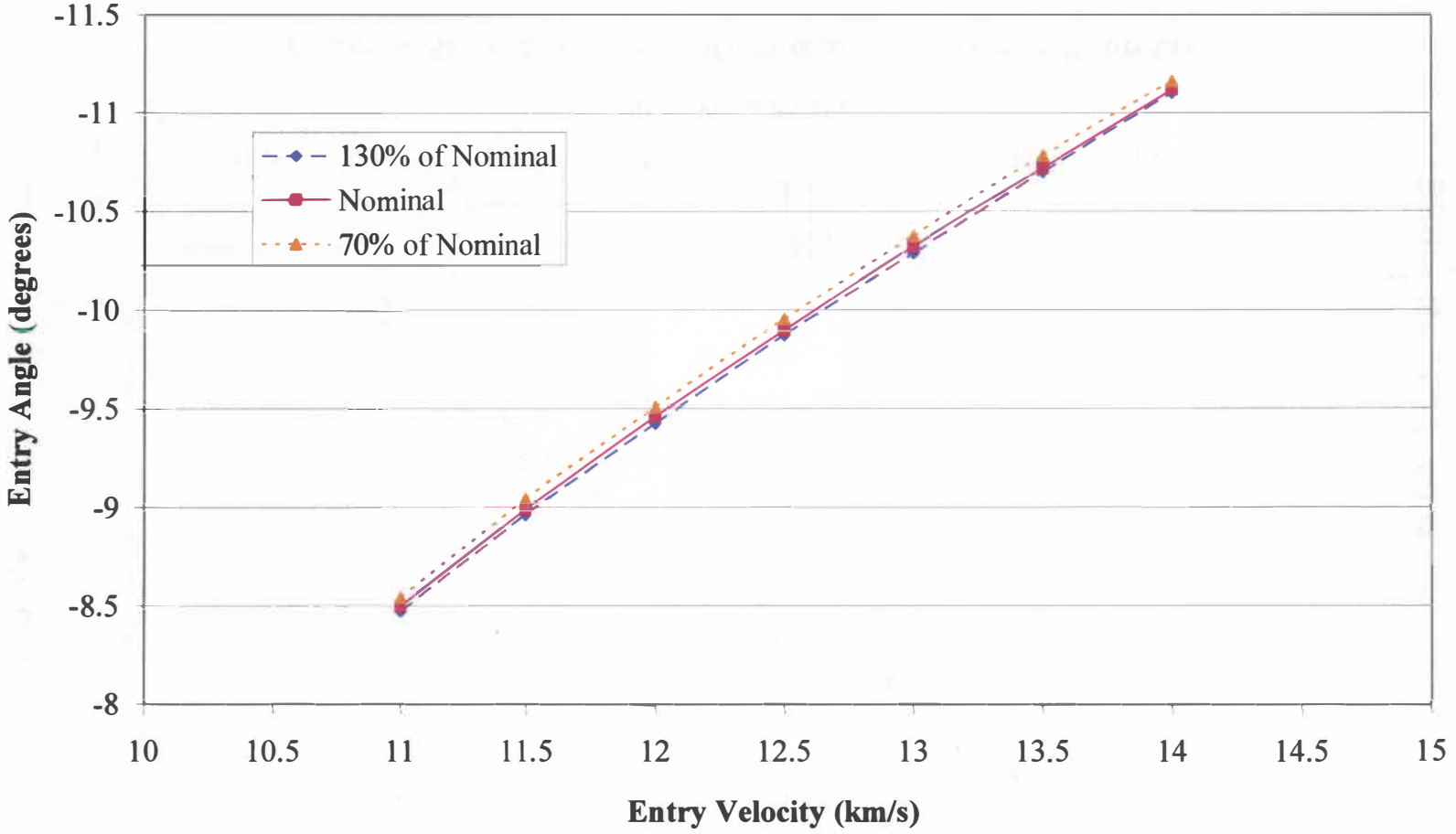

Figure 4-9: Nominal and Off-nominal Undershoot Boundary (no roll maneuvers)

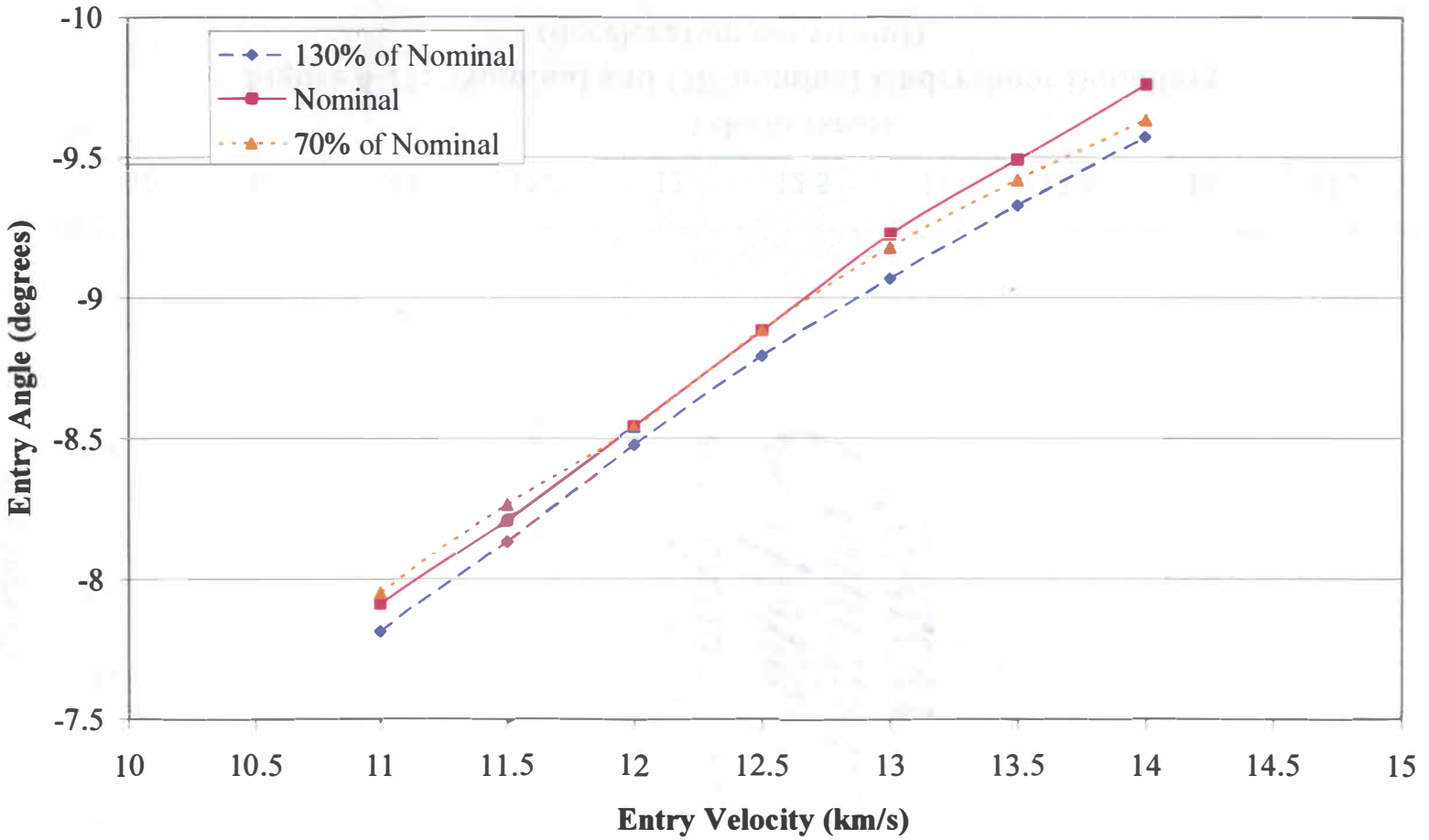

Figure 4-10: Nominal and Off-nominal Undershoot Boundary (targeted periapse)

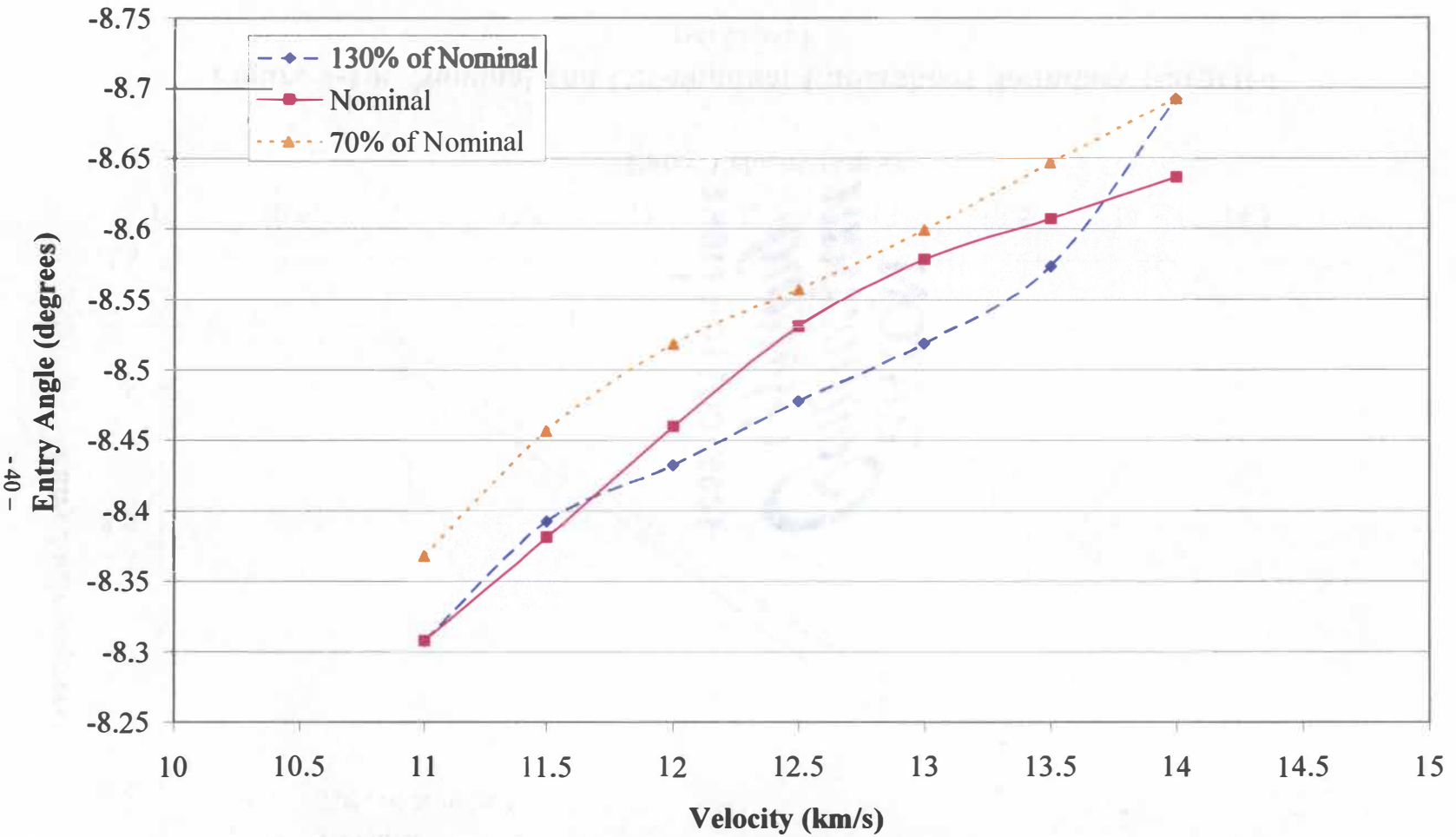

Figure 4-11: Nominal and Off-nominal Undershoot Boundary (deceleration constraint)

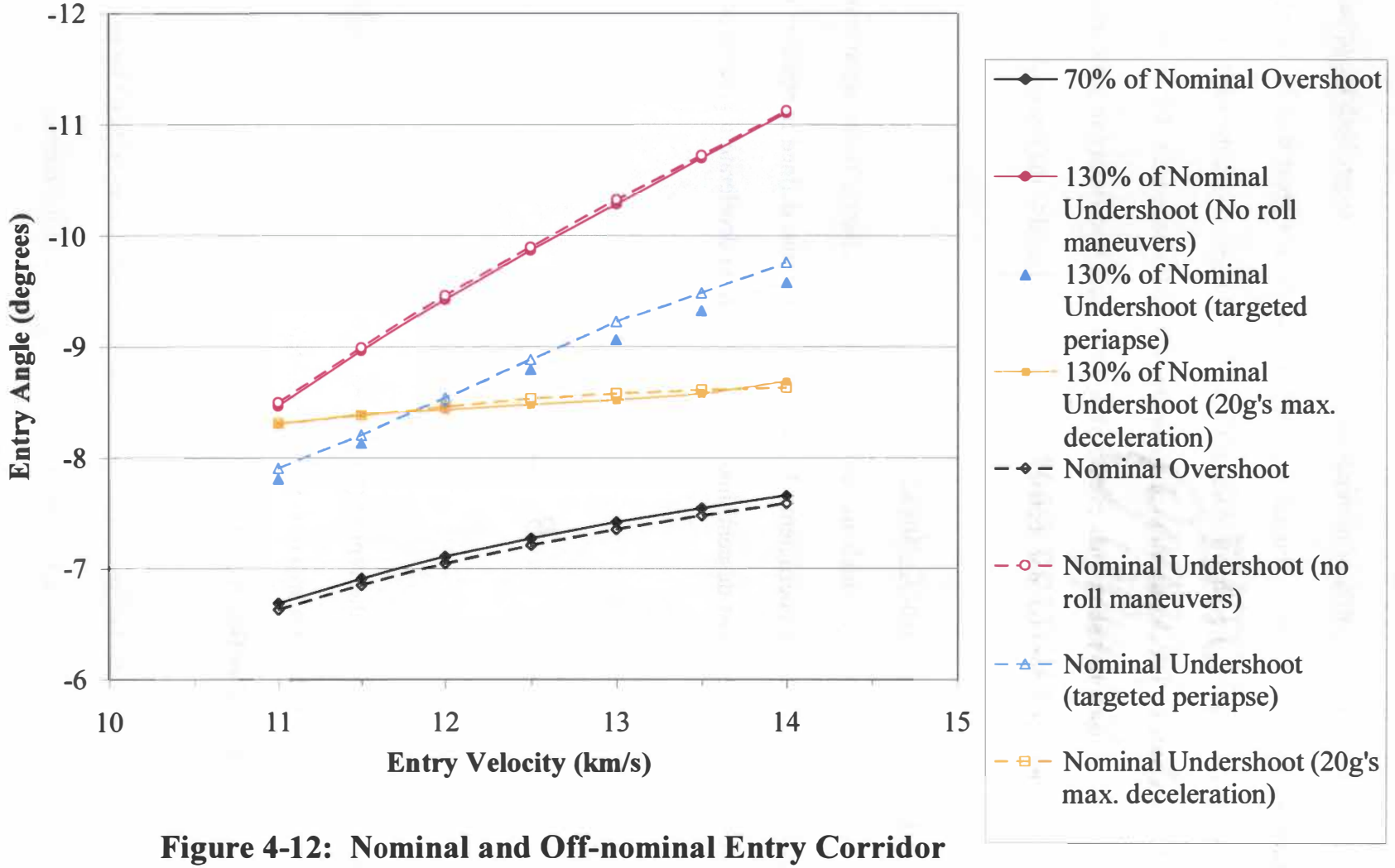

Figure 4-12: Nominal and Off-nominal Entry Corridor

the tolerances, but close enough to allow capture. The same is seen in the 70% of nominal analysis, but the 130% of nominal analysis was able to target both the apoapse and periapse for all velocities. Figure 4-11 appears to show a great deal of variation compared to the other figures, but looking at the scale and Figure 4-12, the variations are actually quite small. The deceleration and apoapse fell within tolerances for all cases in Figure 4-11. These plots show that even with a 30 percent uncertainty in atmospheric density, the entry corridor does not change significantly compared to the nominal case.

Section 4-4 Ballistic Coefficient

Another method by which the entry corridor may change is an aerodynamic property called the ballistic coefficient. The ballistic coefficient, defined in equation (1), reflects how far a body must descend into the atmosphere to decelerate a given amount [26].

(Eqn. 1) $$B^* = \frac{m}{C_D S}$$

where: m = Mass of the vehicle (kilograms)

S = Reference area of the vehicle (meters^2)

C_D = Coefficient of drag

Using the equation 1, the ballistic coefficient for the nominal vehicle is 78.02 kg/m^2. To examine how B^* affects the entry corridor, the reference area of the nominal vehicle was

changed by reducing the radius from 1 meter to 0.75 meters. This represents a B^* that is a 77.78% increase in the original value to 138.7 kg/m^2. An alternate method of changing B^* is to change the mass of the vehicle, but this study was to concentrate on small probes, so the probe was made slightly smaller instead of more massive. The resulting entry corridor seen in Figure 4-13 and compared with the nominal vehicle corridor shows a shift in the corridor with very little change in the width of the entry corridor. The undershoot case was the untargeted periapse with no deceleration constraint.

Section 4-5 Heating Rate Analysis

Vehicles that will enter into an aerocapture trajectory will often be subjected to high heating rates especially at higher entry velocities. Venus complicates this further by having a much denser atmosphere when compared with the other planets. The heating rate defines the materials needed for the heat shield and how thick the heat shield must be to protect the internal mechanisms of the vehicle. If the heat becomes too intense, then the required mass of the thermal protection system may become prohibitive. There are two types of heating that play a part in entry, radiation and convection. At the lower entry speeds, convection is the dominant form of heating, but at higher speeds, this changes to radiation. All heating calculations were performed at the stagnation-point with an effective nose radius of 1.92 meters.

Section 4-5.1 Radiative Heating Rates

Heat from radiation plays a dominant roll in the higher entry velocities, but cannot be neglected for any entry speed. While some work had been done on radiative heating

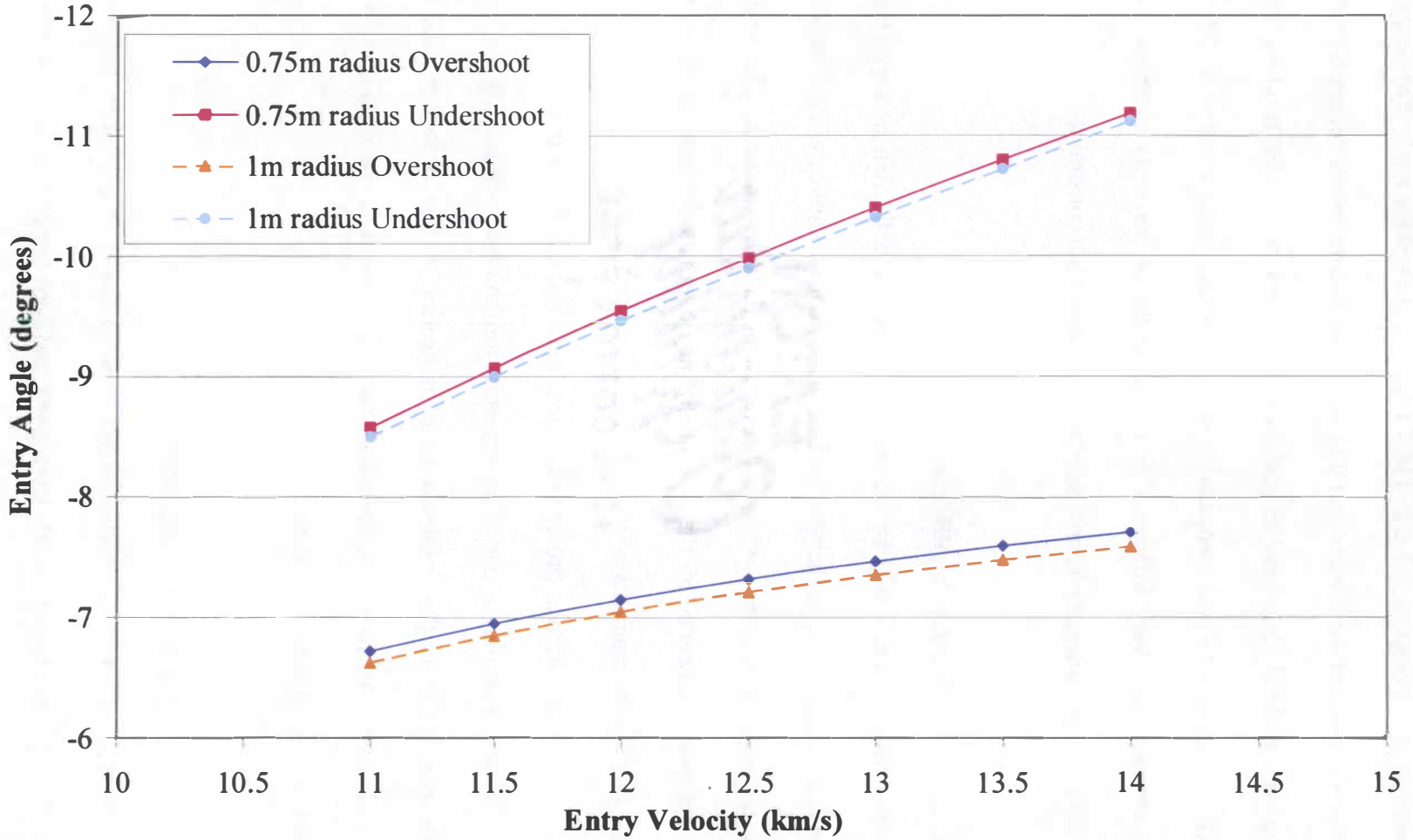

Figure 4-13: Ballistic Coefficient Comparison

in the Venusian atmosphere in the 1970's [24], the equations derived did not encompass the velocities covered in this study. However, more work has recently expanded these equations to cover free-stream velocities up to 12 km/s [25]. Using the set of equations (2-4), radiative heating at the stagnation point was calculated for the entry velocities of 11 km/s through 12.5 km/s. The higher entry velocities produced a peak heating rate outside the 12 km/s maximum for the equations so they were not calculated.

(Eqn. 2)
$$10{,}000 \le V_1 \le 12{,}000 \frac{m}{\text{sec}}$$
$$\dot{q}_r = 3.07 * 10^{-48} V_1^{13.4} \rho_1^{1.2} r_n^{0.49} \frac{W}{cm^2}$$

(Eqn. 3)
$$8{,}000 \le V_1 < 10{,}000 \frac{m}{\text{sec}}$$
$$\dot{q}_r = 1.22 * 10^{-16} V_1^{5.5} \rho_1^{1.2} r_n^{0.49} \frac{W}{cm^2}$$

(Eqn. 4)
$$V_1 < 8{,}000 \frac{m}{\text{sec}}$$
$$\dot{q}_r = 3.33 * 10^{-34} V_1^{10.0} \rho_1^{1.2} r_n^{0.49} \frac{W}{cm^2}$$

where: V_1 = Free-stream velocity

ρ_1 = Free-stream density

r_n = Effective nose radius

An example of the radiative heating curve at 12 km/s entry speed is shown in Figure 4-14. It clearly shows that while radiative heating is fairly small, about 35 W/cm^2 maximum, for the overshoot, it is much larger for the undershoot where it is closer to 270

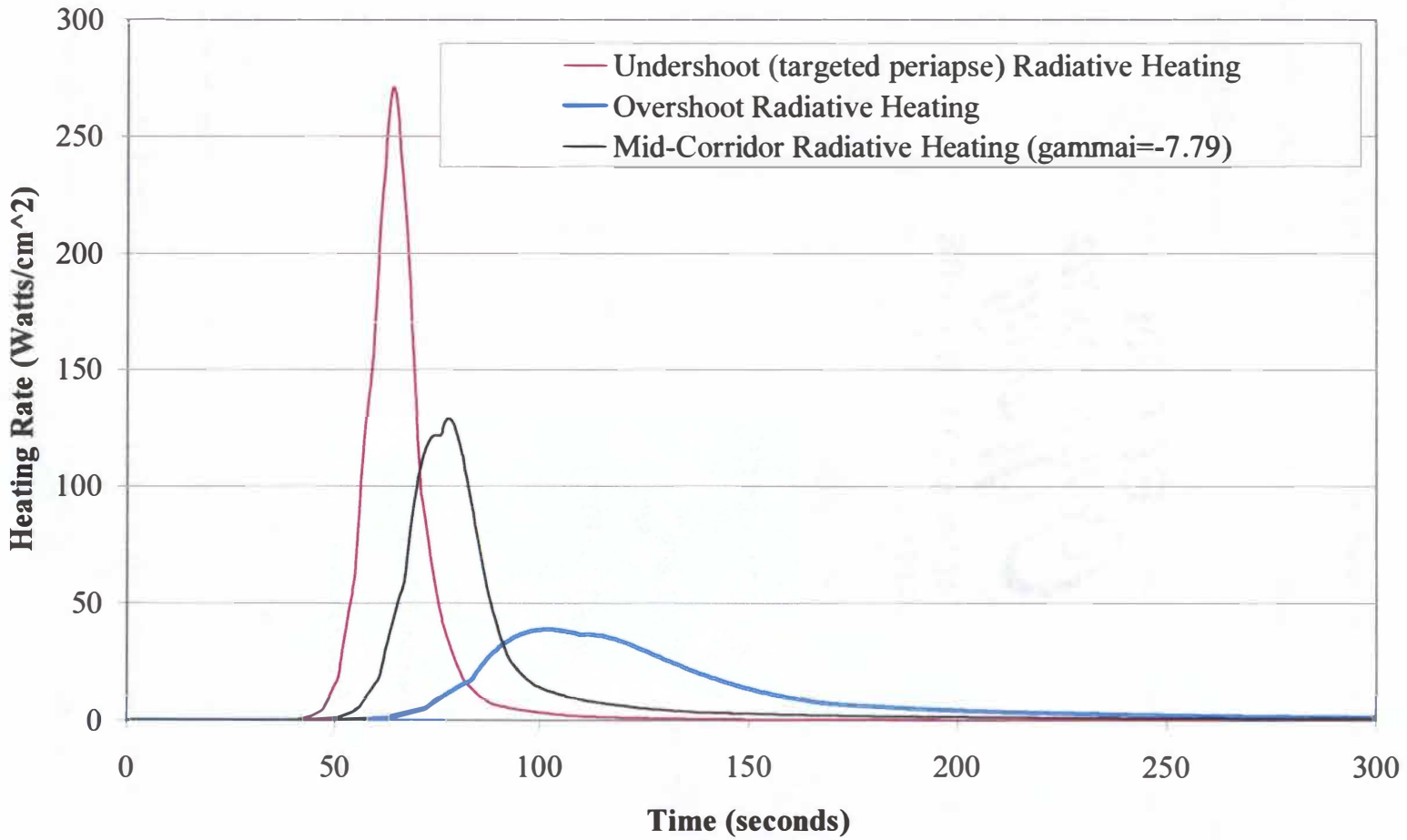

Figure 4-14: Stagnation-point Radiative Heating for the Nominal Vehicle at 12km/s

W/cm^2 at the maximum. The mid-corridor trajectory is plotted for reference to show what an actual mission might encounter. The maximum radiative heating rate for the lower entry speeds is shown on Figure 4-15. Note that the maximum heating rate encounters exponential growth as the entry velocity increases.

Section 4-5.2 Convective Heating Rates

Convective heating comprises the rest of the heat that is encountered by the vehicle during entry. As stated earlier, it becomes the dominant form of heating for the lower entry speeds. Equation 5 shows the relation used to determine the convective heating rate at the stagnation point [6]. Note that it is dependant on free stream enthalpy and wall enthalpy. The wall enthalpy is found from the radiative and convective heating rates, and the free stream enthalpy is assumed to be constant because the only point where the free stream enthalpy is important is near the point of maximum heating. Otherwise the value of h_w / h_T is very small and can be neglected.

(Eqn. 5)
$$\dot{q}_{r_{conv}} = 1.4 * 10^{-8} \left(\frac{\rho_1}{r_n} \right)^{0.5} V_1^{3.04} \left(1 - \frac{h_w}{h_T} \right) \frac{W}{cm^2}$$

where: V_1 = Free-stream velocity

ρ_1 = Free-stream density

r_n = Effective nose radius

h_w = Wall enthalpy

h_T = Total enthalpy

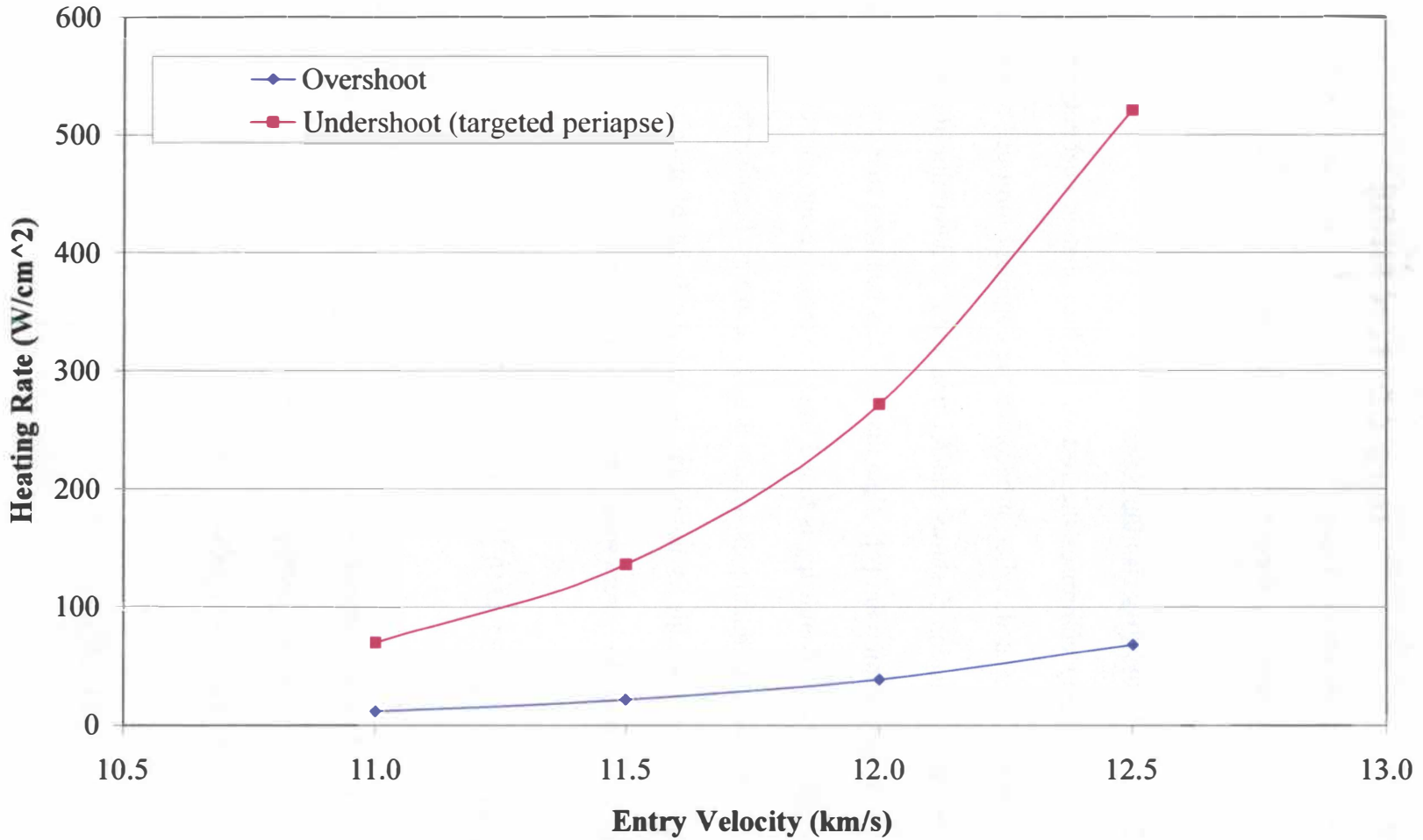

Figure 4-15: Peak Stagnation-point Radiative Heating Rates

Because the wall enthalpy is dependant on the radiative heating, the convective heating rate was only calculated on the trajectories with entry speeds up to 12.5 km/s. Convective heating for the 12 km/s trajectory is shown in Figure 4-16 for the overshoot, mid-corridor and targeted periapse undershoot. Figure 4-17 shows the peak convective heating rate for the entry velocities up to 12.5 km/s.

Section 4-5.3 Total Heating Rates

The total heating rates for any given time are found by adding the radiative and convective heating rates. While either one of the individual heating rates may be dominant, neither one should be neglected. The maximum total heating rate for each trajectory was found using the respective equations and plotted in Figure 4-18. It clearly shows an exponential growth of the maximum total heating rate for the undershoot. However, the overshoot remains relatively small in magnitude, so higher entry speeds may be possible, but the total heating rate may be an additional constraint, further reducing the corridor. Finally, the total heating rate is plotted for the 12 km/s targeted periapse undershoot, mid-corridor and overshoot trajectories in Figure 4-19.

Section 4-5.4 Total Integrated Heat Load

The total heat load encountered by the vehicle was determined by integrating the heating rate data over the course of the trajectory. The trapezoidal method was used for simplicity and the time step was sufficiently small to keep errors to a minimum. The results are displayed in Figure 4-20. The total heat load for the overshoot is higher because, while it is not subjected to the highest heating rates, it experiences heating over

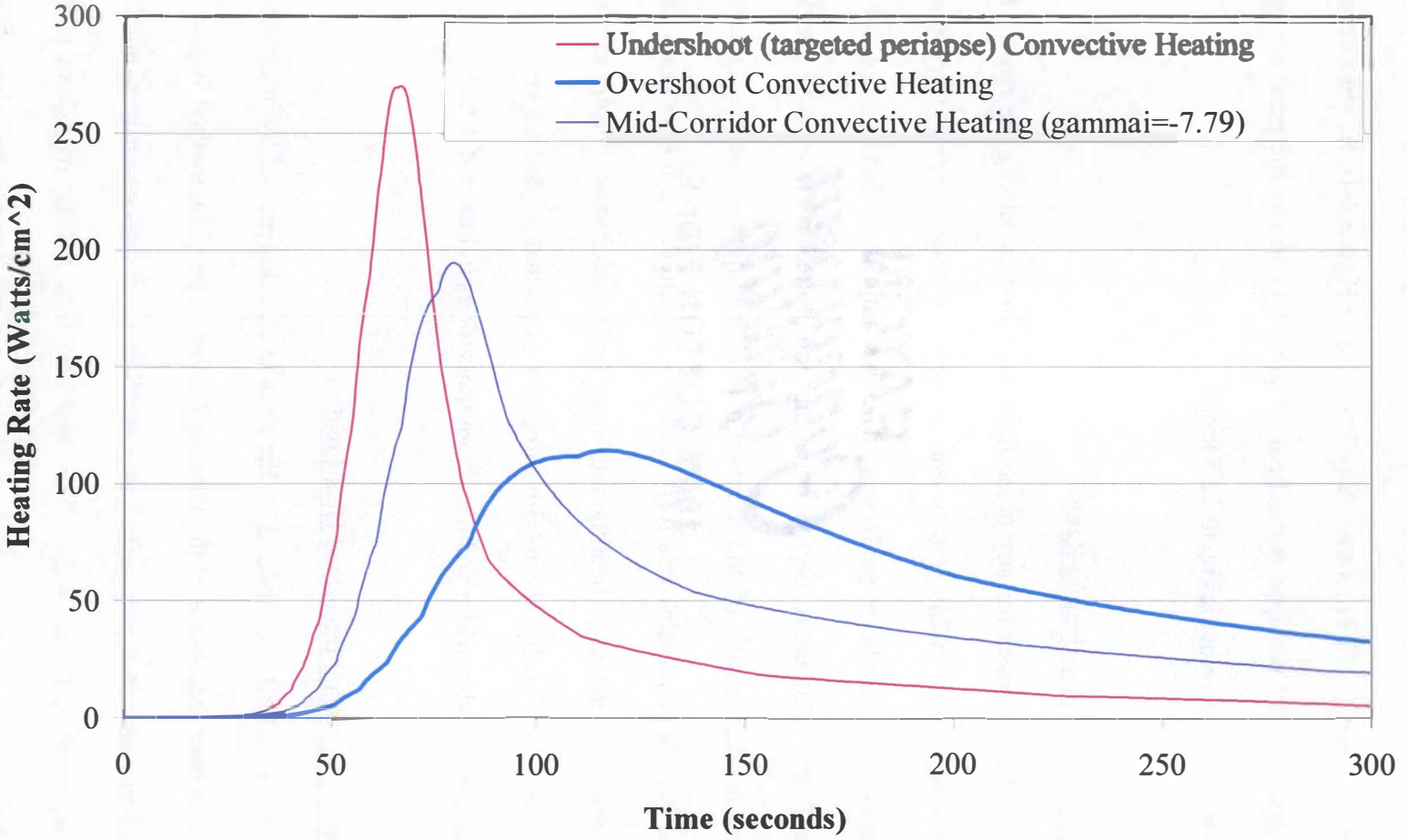

Figure 4-16: Stagnation-point Convective Heating for the Nominal Vehicle at 12 km/s

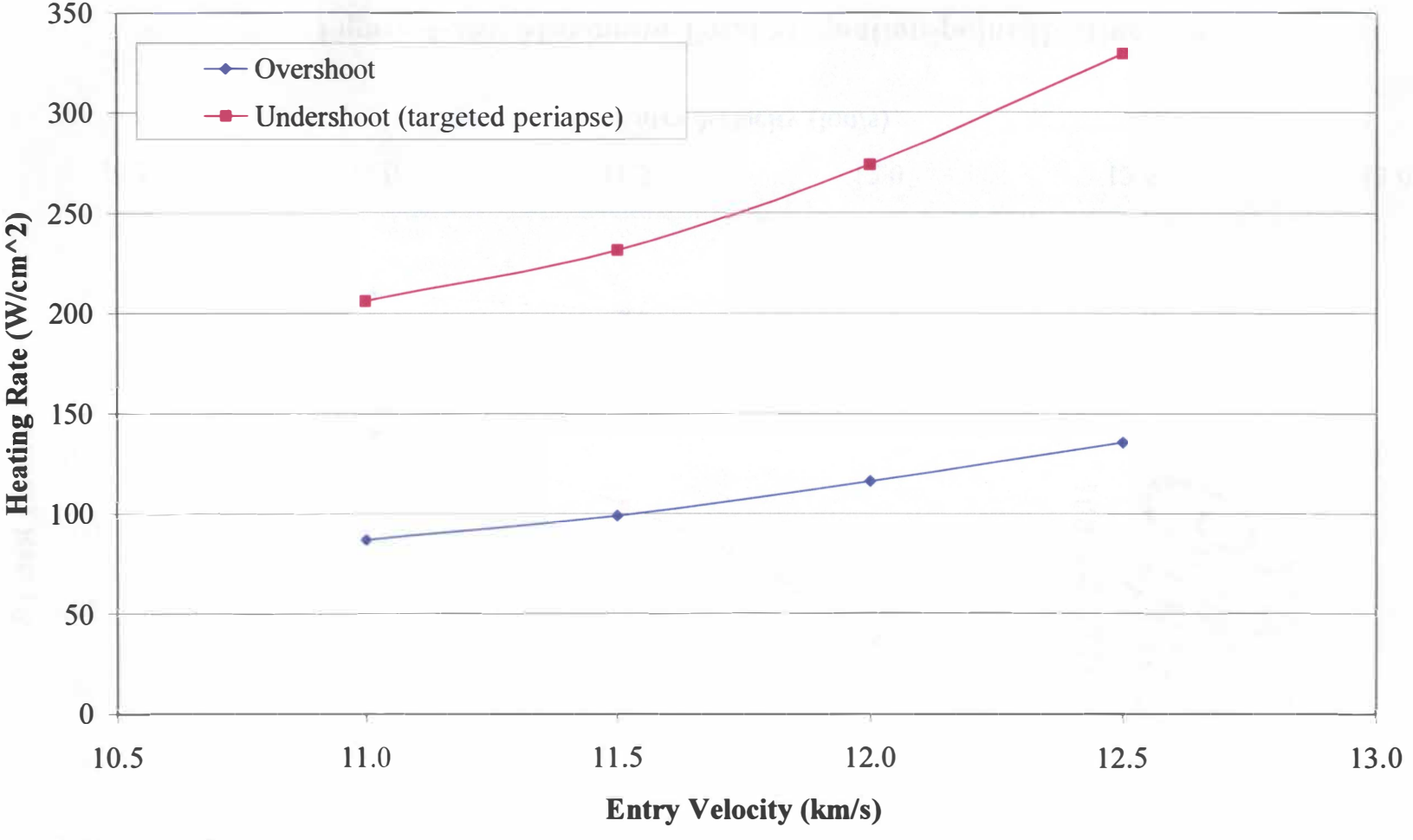

Figure 4-17: Peak Stagnation-point Convective Heating Rates

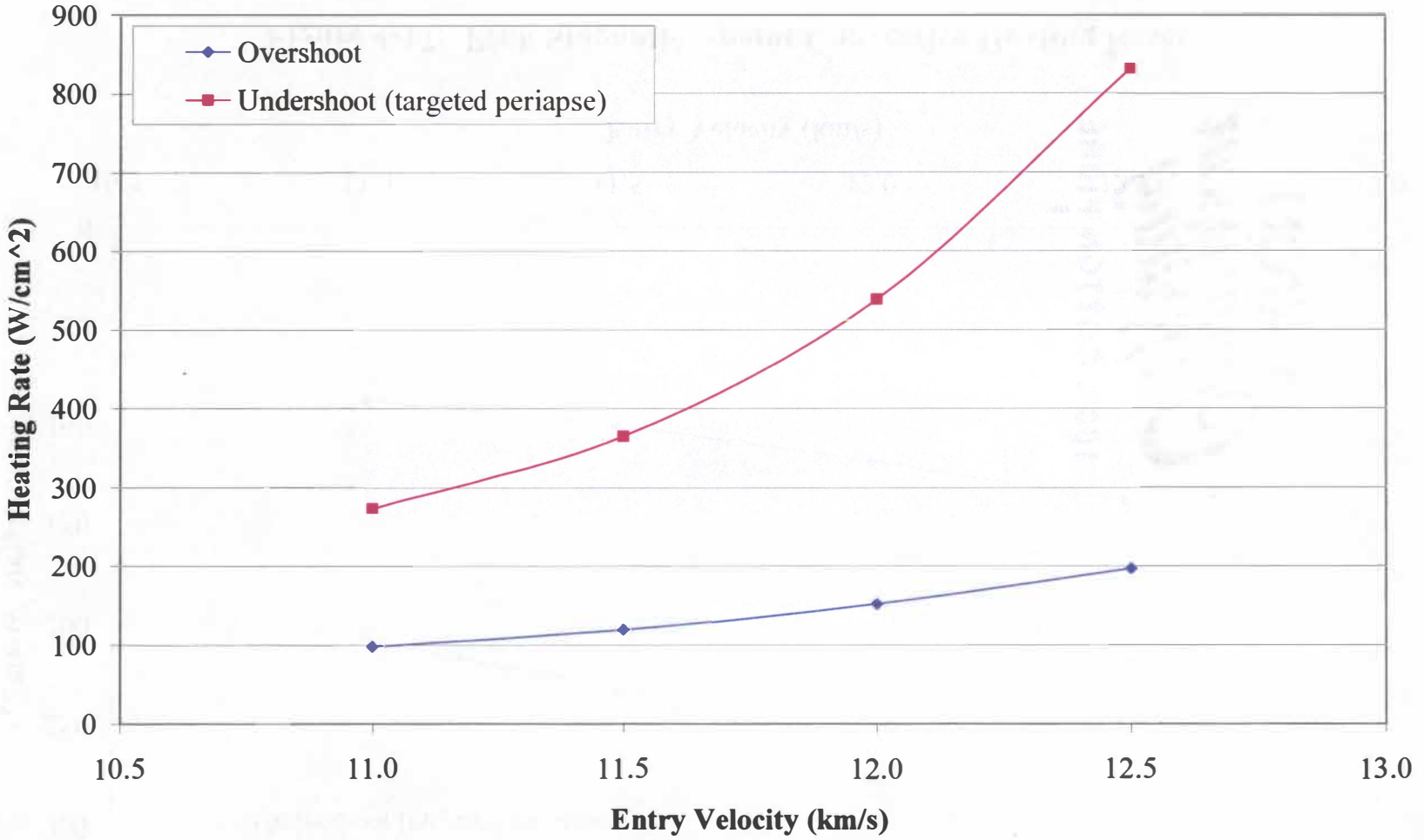

Figure 4-18: Maximum Total Stagnation-point Heating Rate

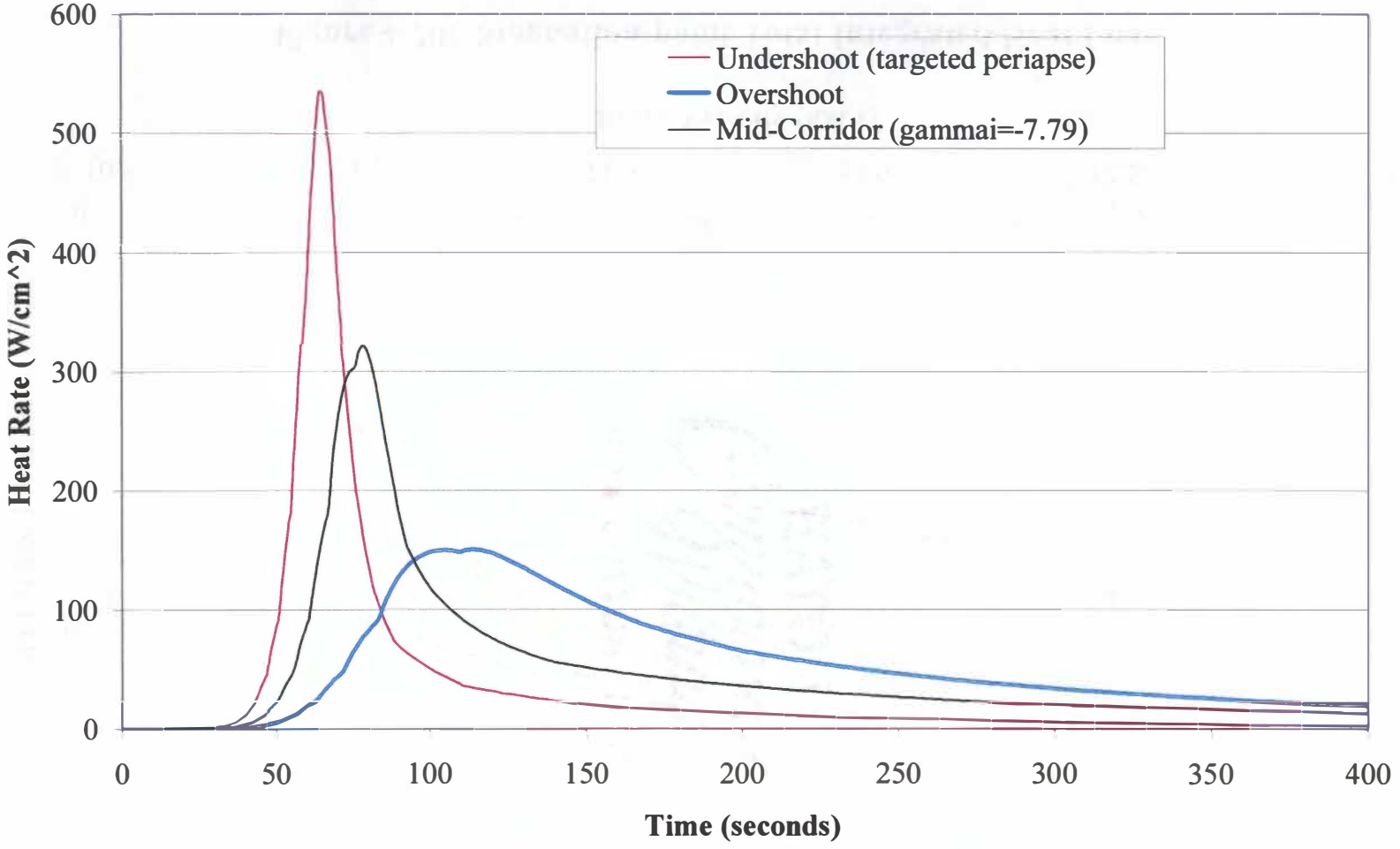

Figure 4-19: Total Stagnation-point Heating Rate for the Nominal Vehicle at 12 km/s

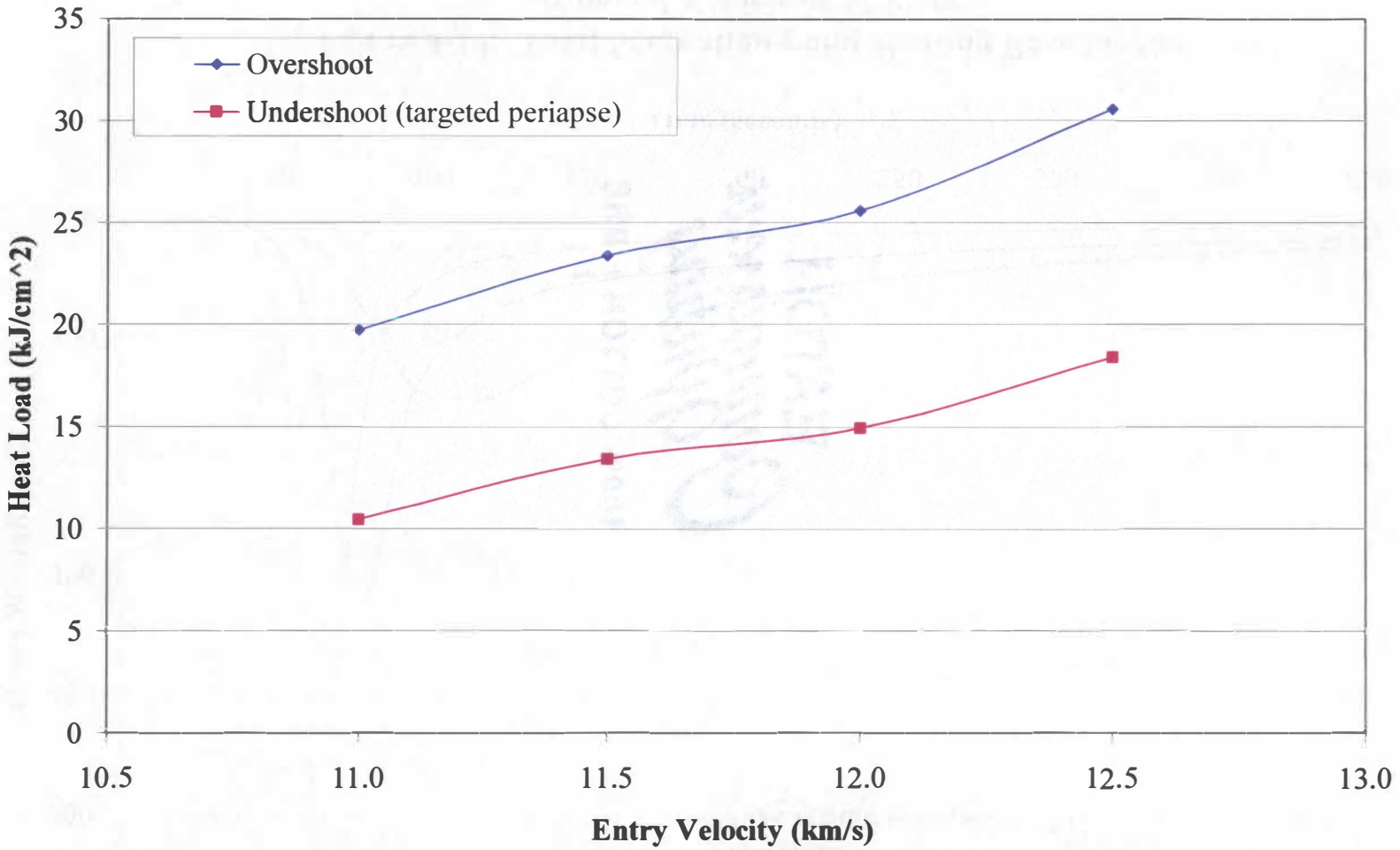

Figure 4-20: Stagnation-point Total Integrated Heat Load

a much longer period of time. Also, the total heat load for a mid-corridor trajectory at 12 km/s was calculated to be 21.44 kJ/cm^2.

Section 4-6 Orbit Circularization

In order for the orbit to become stable, the periapse must be raised out of the atmosphere. If this was not done, then the vehicle would crash onto the planet surface following the next orbit. This is accomplished by performing a rocket burn at the apoapse and another smaller burn to correct the error in trajectory at the new periapse. Equation 6 [26] shows how the delta V at the apoapse is determined using the apoapse and periapse from the trajectory data. Equation 7 shows the ΔV for the new periapse to correct for the error in the apoapse.

(Eqn. 6) $$\Delta V = \sqrt{\frac{\mu}{R+A}} - \sqrt{\frac{2\mu}{R+A} - \frac{2\mu}{2R+A+P}}$$

(Eqn. 7) $$\Delta V = \sqrt{\frac{2\mu}{R+T} - \frac{2\mu}{2R+A+T}} - \sqrt{\frac{\mu}{R+T}}$$

where: μ = Gravitational parameter (Gravitational constant * mass of planet)

R = Radius of planet

A = Apoapse altitude

P = Periapse altitude

T = Target orbit altitude

Now it becomes apparent why the undershoot with no roll maneuvers is not a viable trajectory. As seen in Tables 4-5 and compared to Table 4-6 through 4-8, the delta V required to circularize the orbit at 407 kilometers is significantly larger than the other trajectories. To put this in perspective, the fuel required for both ΔV's are calculated using the rocket equation listed as equation 8 [26]. The I_{sp} used for the calculations is that of a liquid hydrogen and liquid oxygen engine (I_{sp} = 391s), hydrazine (I_{sp} = 205s), and RP-1 and liquid oxygen (I_{sp} = 300s) [27]. Other hydrocarbon liquid fuel engines have different I_{sp}'s, but these values give a good range over the available fuels. Remembering that the vehicle has an initial mass of 300 kilograms, Tables 4-5 through 4-8 show how much of that mass must be devoted to fuel in order to attain the target orbit after aerocapture.

(Eqn. 8) $$\Delta V = I_{sp} g \ln\left[\frac{m_0}{m}\right]$$

where: I_{sp} = Specific impulse of the engine

g = Gravity of the planet (8.87 m/s^2 for Venus)

m_0 = Initial mass of vehicle

m = Final mass of vehicle

The obvious implications of the fuel required is that the undershoot with no roll maneuvers requires far too much fuel to be used as a trajectory. When eight to fifteen percent of the total vehicle weight is fuel, the trajectory is not saving the weight it should. Also, the engine itself is not taken into account in the equation, but is deemed a constant

Table 4-5: Undershoot (no roll maneuvers) Delta V and Fuel Mass requirements

			Delta V			Fuel mass required (kg)		
Velocity (km/s)	Apoapse(km)	Periapse(km)	for Apoapse (m/s)	for Periapse (m/s)	Total (m/s)	Isp=205	Isp=300	Isp=391
11	413.05	-651.74	322.38	-1.66	324.04	48.97	34.40	26.76
11.5	414.53	-791.48	370.39	-2.07	372.46	55.57	39.18	30.55
12	412.01	-944.01	425.76	-1.38	427.14	62.81	44.49	34.76
12.5	416.23	-1075.10	473.00	-2.53	475.53	69.04	49.09	38.44
13	413.10	-1229.70	533.04	-1.67	534.72	76.43	54.61	42.86
13.5	416.69	-1355.50	581.68	-2.66	584.34	82.45	59.15	46.52
14	412.20	-1513.00	647.46	-1.43	648.88	90.04	64.92	51.19

Table 4-6: Overshoot Delta V and Fuel Mass requirements

			Delta V			Fuel mass required (kg)		
Velocity (km/s)	Apoapse(km)	Periapse(km)	for Apoapse (m/s)	for Periapse (m/s)	Total (m/s)	Isp=205	Isp=300	Isp=391
11	411.04	113.61	81.81	-1.11	82.92	13.37	7.91	7.09
11.5	412.73	113.60	81.34	-1.57	82.91	13.37	7.91	7.09
12	412.06	113.60	81.53	-1.39	82.92	13.37	7.91	7.09
12.5	415.54	113.59	80.56	-2.34	82.91	13.37	7.91	7.09
13	412.65	113.60	81.36	-1.55	82.91	13.37	7.91	7.09
13.5	410.85	113.61	81.86	-1.06	82.92	13.37	7.91	7.09
14	411.62	113.60	81.65	-1.27	82.92	13.37	7.91	7.09

Table 4-7: Undershoot (targeted periapse) Delta V and Fuel Mass requirements

			Delta V			Fuel mass required (kg)		
Velocity (km/s)	Apoapse(km)	Periapse(km)	for Apoapse (m/s)	for Periapse (m/s)	Total (m/s)	Isp=205	Isp=300	Isp=391
11	407.43	104.38	85.50	-0.12	85.62	13.80	9.50	7.32
11.5	414.98	109.86	81.80	-2.19	83.99	13.54	9.32	7.18
12	416.03	109.91	81.50	-2.48	83.97	13.54	9.32	7.18
12.5	419.73	108.58	80.85	-3.49	84.34	13.60	9.36	7.21
13	410.71	108.19	83.48	-1.02	84.50	13.62	9.38	7.22
13.5	383.26	105.19	91.97	6.53	98.51	15.82	10.90	8.40
14	379.71	103.49	93.45	7.51	100.97	16.20	11.17	8.61

Table 4-8: Undershoot (deceleration constraint) Delta V and Fuel Mass requirements

			Delta V			Fuel mass required (kg)		
Velocity (km/s)	Apoapse(km)	Periapse(km)	for Apoapse (m/s)	for Periapse (m/s)	Total (m/s)	Isp=205	Isp=300	Isp=391
11	407.92	-152.55	162.23	-0.25	162.48	25.64	17.77	13.73
11.5	404.48	90.34	90.42	0.69	91.11	14.66	10.10	7.78
12	406.40	112.02	83.56	0.16	83.73	13.50	9.29	7.16
12.5	403.96	113.39	83.84	0.84	84.68	13.65	9.40	7.24
13	414.15	113.53	80.97	-1.96	82.93	13.37	9.21	7.09
13.5	405.83	113.58	83.26	0.32	83.59	13.48	9.28	7.14
14	407.14	113.58	82.90	-0.04	82.94	13.38	9.21	7.09

throughout all the trajectories. Liquid hydrogen and liquid oxygen is one of the more efficient fuels available, but requires cryogenic storage. Hydrazine is more commonly used in long term missions, but is very volatile. To determine the best fuel, both weight and cost of the engine and fuel must be considered.

Chapter 5

Alternate Angle of Attack

To give another reference the nominal Apollo configuration entry corridor was calculated using an alternate angle of attack, AOA. The purpose was to analyze how a lower L/D vehicle performed in the Venus atmosphere and compare the entry corridors. The aerodynamic constants were calculated using NASA's IDS website and the AOA was found for an L/D of approximately 0.20. Using the Apollo AOA convention defined earlier, this turned out to be 166.7 degrees with a coefficient of lift of 0.2573 and a coefficient of drag of 1.285. Although it was shown earlier that the IDS website had some error (<10%), this was not found to be a problem for a preliminary study. The entry corridor for the alternate angle of attack can be found on Figure 5-1.

The nature of the lower L/D did not allow the vehicle to target the 112 km periapse used for the nominal AOA. Thus, a slightly lower periapse of 107 km was used. In comparison to the nominal AOA, POST had a much easier time hitting the targets for all runs with all trajectories falling within the prescribed tolerances. Because the vehicle did not have as much lifting capability as the nominal AOA in these runs, the periapse for the undershoot without roll maneuvers were not as severe, but they were still sufficiently low to prohibit using that trajectory, as seen in Tables 5-1 through 5-4. Also calculated were the delta V requirements and fuel mass requirements for the same fuels used for the nominal vehicle. To compare the heating rates between the two angles of attack, the total

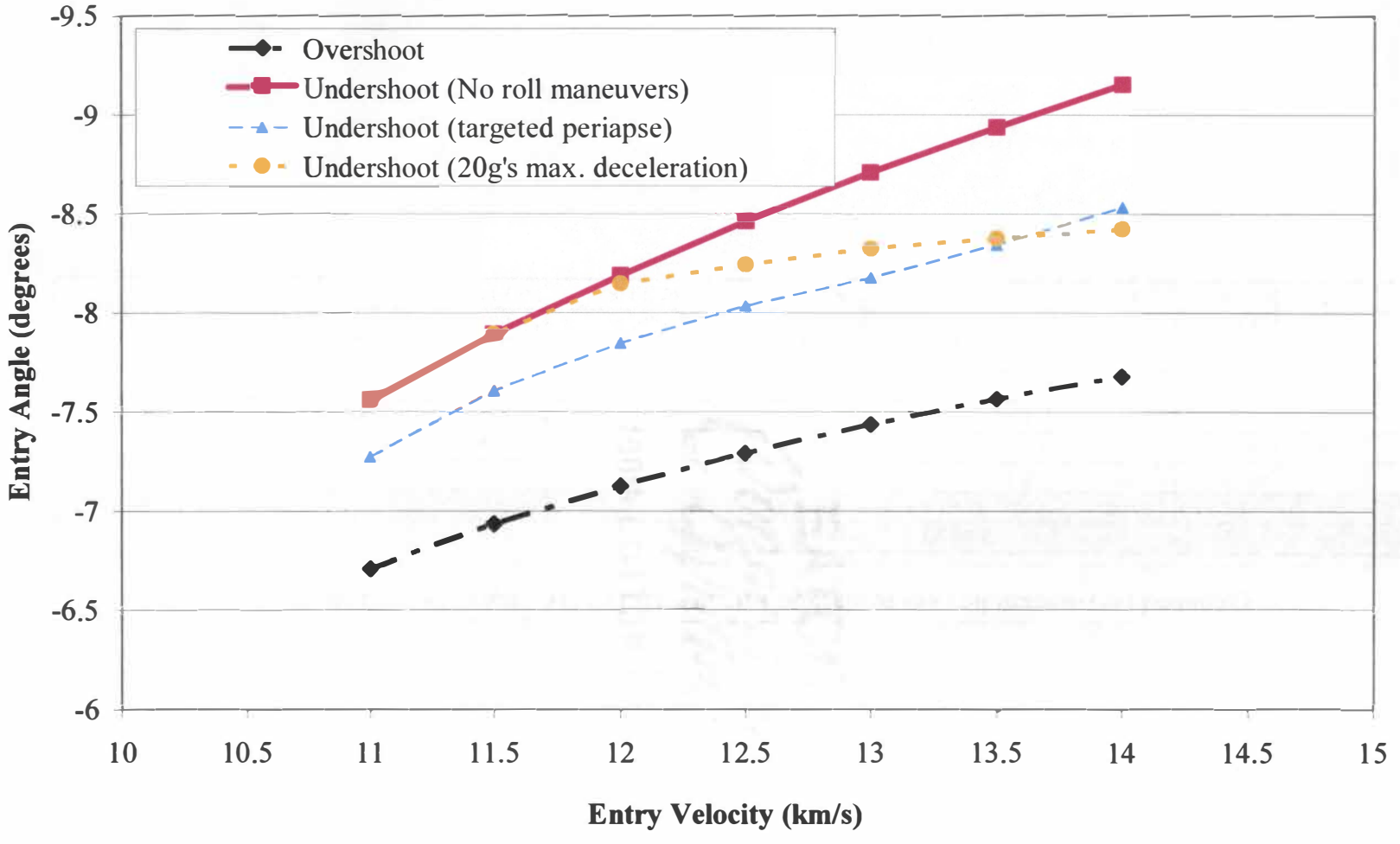

Figure 5-1: Alternate Angle of Attack (L/D = 0.20) Entry Corridor

Table 5-1: Alternate AOA (L/D = 0.20) Undershoot (no roll maneuvers) boundary

				Delta V			Fuel mass required (kg)		
Velocity (km/s)	Entry Angle (deg)	Apoapse(km)	Periapse(km)	for Apoapse (m/s)	for Periapse (m/s)	Total (m/s)	Isp=205	Isp=300	Isp=391
11	-7.559002293	413.30	-203.43	176.42	-1.73	178.15	28.00	16.73	15.02
11.5	-7.892079489	409.56	-216.99	181.69	-0.70	182.39	28.63	17.12	15.37
12	-8.187938585	418.50	-306.25	207.19	-3.15	210.34	32.77	19.65	17.65
12.5	-8.461327345	408.22	-376.02	232.39	-0.34	232.72	36.04	21.67	19.47
13	-8.709362271	416.19	-421.36	244.77	-2.52	247.30	38.15	22.97	20.65
13.5	-8.937866909	420.41	-470.04	259.46	-3.68	263.13	40.42	24.38	21.92
14	-9.152681763	415.97	-533.29	281.62	-2.46	284.09	43.39	26.23	23.59

Table 5-2: Alternate AOA (L/D = 0.20) Overshoot Boundary

				Delta V			Fuel mass required (kg)		
Velocity (km/s)	Entry Angle (deg)	Apoapse(km)	Periapse(km)	for Apoapse (m/s)	for Periapse (m/s)	Total (m/s)	Isp=205	Isp=300	Isp=391
11	-6.705777468	414.78	107.86	82.44	-2.13	84.58	13.63	8.06	7.23
11.5	-6.930750944	421.14	107.88	80.66	-3.88	84.54	13.63	8.06	7.22
12	-7.123401281	410.49	107.80	83.65	-0.96	84.61	13.64	8.07	7.23
12.5	-7.290056842	414.98	107.82	82.40	-2.19	84.59	13.64	8.06	7.23
13	-7.435443872	418.10	107.84	81.52	-3.04	84.57	13.63	8.06	7.23
13.5	-7.563211815	419.57	107.83	81.12	-3.45	84.56	13.63	8.06	7.23
14	-7.676168036	415.49	107.80	82.26	-2.33	84.59	13.64	8.06	7.23

Table 5-3: Alternate AOA (L/D = 0.20) Undershoot (targeted periapse) Boundary

			Delta V			Fuel mass required (kg)		
Velocity (km/s)	Apoapse(km)	Periapse(km)	for Apoapse (m/s)	for Periapse (m/s)	Total (m/s)	Isp=205	Isp=300	Isp=391
11	420.60	104.89	81.68	-3.73	85.41	13.77	8.14	7.30
11.5	416.20	102.31	83.66	-2.52	86.19	13.89	8.21	7.36
12	410.55	103.42	84.91	-0.97	85.89	13.84	8.19	7.34
12.5	419.11	105.07	82.05	-3.32	85.37	13.76	8.14	7.29
13	412.34	106.36	83.56	-1.46	85.02	13.70	8.10	7.27
13.5	414.10	106.55	83.01	-1.95	84.96	13.69	8.10	7.26
14	409.65	106.20	84.35	-0.73	85.08	13.71	8.11	7.27

Velocity (km/s)	Entry Angle (deg)	Time to Roll (sec)
11	-7.271011802	103.807
11.5	-7.606729885	94.9646789
12	-7.844680585	86.97084653
12.5	-8.034438695	80.71111436
13	-8.17595412	75.53564459
13.5	-8.344793145	70.7685307
14	-8.535480267	66.35828096

Table 5-4: Alternate AOA (L/D = 0.20) Undershoot (deceleration constraint) Boundary

			Delta V			Fuel mass required (kg)		
Velocity (km/s)	Apoapse(km)	Periapse(km)	for Apoapse (m/s)	for Periapse (m/s)	Total (m/s)	Isp=205	Isp=300	Isp=391
11	413.30	-203.43	176.42	-1.73	178.15	28.00	16.73	15.02
11.5	409.56	-216.99	181.69	-0.70	182.39	28.63	17.12	15.37
12	427.51	-94.72	139.08	-5.62	144.70	22.95	13.66	12.26
12.5	412.94	74.23	92.78	-1.63	94.41	15.18	8.99	8.06
13	401.11	100.66	88.34	1.62	89.96	14.48	8.57	7.68
13.5	407.60	106.03	84.97	-0.17	85.14	13.72	8.12	7.27
14	420.62	107.27	80.99	-3.73	84.72	13.66	8.08	7.24

Velocity (km/s)	Entry Angle (deg)	Time to Roll (sec)
11	-7.559002293	N/A
11.5	-7.892679489	N/A
12	-8.146898535	91.14949533
12.5	-8.244271435	79.67902832
13	-8.324681832	74.61993775
13.5	-8.376991613	70.58062081
14	-8.424087375	66.99940281

heat rate at 12 km/s was calculated for the overshoot and targeted periapse undershoot and plotted in Figure 5-2. Table 5-5 shows the difference in total integrated heat load in J/cm^2 at the same 12 km/s entry trajectories.

Table 5-5: Total Integrated Heat Load Comparison at the 12 km/s Entry Speed for the Nominal and Low L/D AOA.

AOA (deg)	L/D	Overshoot (J/cm^2)	Undershoot (targeted periapse) (J/cm^2)
156.7	0.35	25563	14934
166.7	0.2	21050	15665

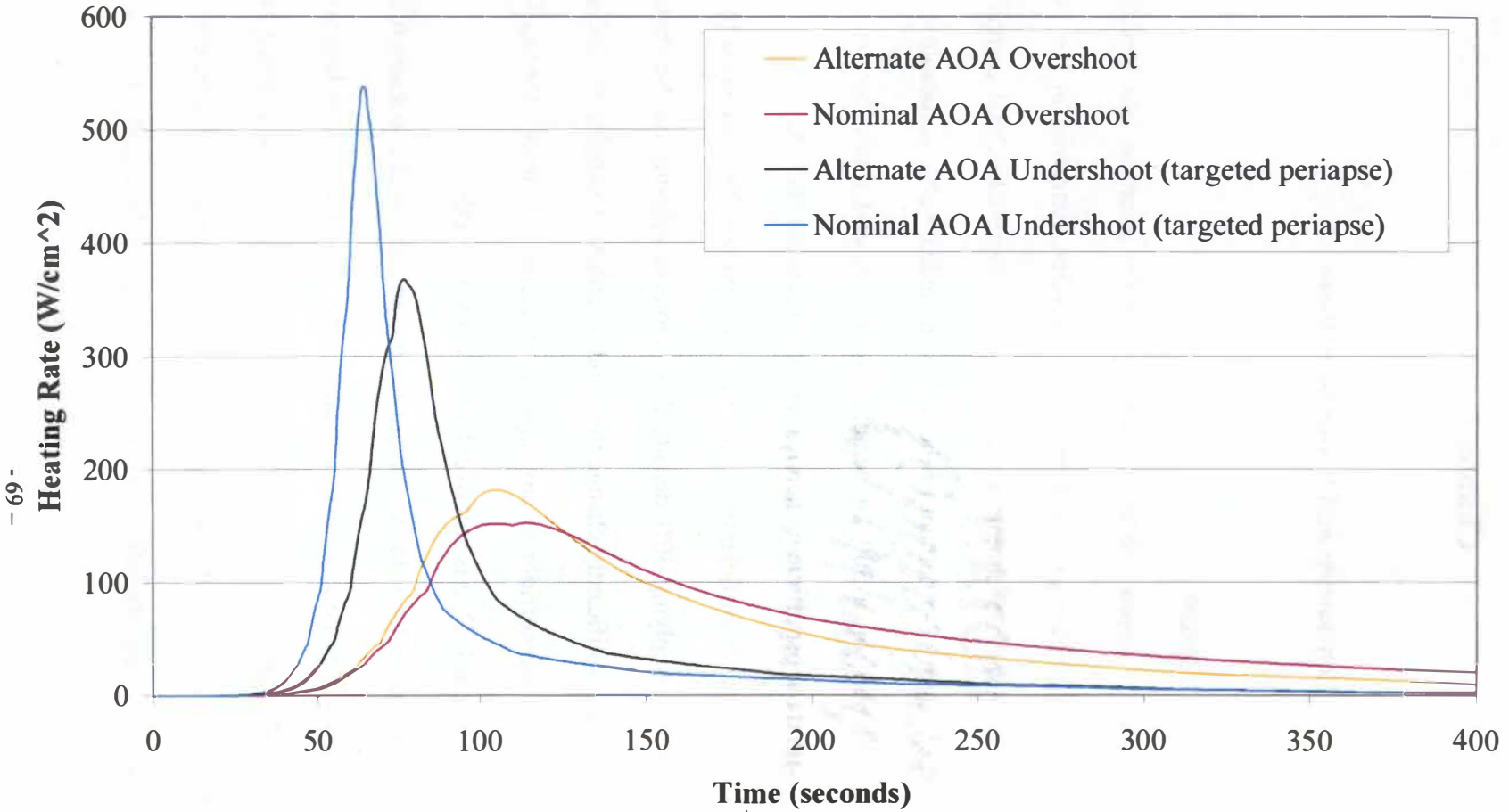

Figure 5-2: Comparison of Total Heating Rates for Two Angles of Attack
(Nominal: AOA=156.7 Degrees, L/D = 0.35)
(Alternate: AOA=166.7 Degrees, L/D =0.20)

Chapter 6

Conclusions and Recommendations

Section 6-1 Conclusions

Overall, aerocapture appears to be a viable option for insertion into Venusian orbit. The possible weight savings could be enormous when compared to the mass required for an orbital burn to accomplish the same task. Optimal orbital correction burns are on the order of only 3-5 percent of the total vehicle mass after aerocapture. In comparison an orbital burn on a 300 kg vehicle requires several times that mass to capture into orbit with the most efficient chemical propellants available today.

The entry corridors are sufficiently large to allow capture with some error in the interplanetary trajectory. Applying 30% density dispersions or entering on the daytime side of the planet did not significantly change the window either. Changing the ballistic coefficient did not affect the corridor to any significant degree. Although the corridor reduces in size for a reduced L/D, it is still over half a degree in width.

However, the higher entry velocities might require an additional constraint due to the exponential growth of the peak stagnation heating rate. Total integrated heat loads for the lower entry velocities were comparable to those predicted for the manned Mars mission Earth return at 12.5 km/s [4], and peak stagnation heating rates for a mid-corridor trajectory at 12 km/s were near the values experienced by the Apollo moon missions. In

conclusion, aerocapture appears to be viable for future missions to Venus, but further study must be conducted to confirm this.

Section 6-2 Recommendations for Future Work

Preliminary studies must make a number of assumptions about the problem in question. In this case, an Apollo configuration was used for the entry vehicle, with the size and mass based off the Pioneer Venus large probe. Also, the orbit was based off current low Earth orbit, due to the size similarity between Earth and Venus. The ballistic coefficient was only varied once and no heating calculations were performed on the trajectories output by this variation.

A variety of vehicles should be examined, possibly including the Mars Pathfinder entry vehicle or one of the Pioneer Venus probes on a non-ballistic entry. These are not the only configurations possible, but these have been used in missions before. If NASA decides in the near future to send another mission to Venus, the mission objectives will help determine the vehicle size and weight by the instruments required for the mission.

Inclination and longitude of the ascending node of the orbit were neglected throughout this study, but may not be able to be neglected in an actual mission. If a polar orbit similar to Magellan is required, then an inclination of 90 degrees must be achieved. The same can be said for an equatorial orbit with an inclination of 0 degrees. Inclination on Venus is not as important as at Earth since there is no need to rendezvous with the International Space Station, or enter an orbit that avoids other satellites, but may be required for some specific data on the Venusian gravity or other reason.

The ballistic coefficient should be examined further to determine how it affects heating. It has been shown that increases in the ballistic coefficient can increase the heating rates [4]. While the heating rates and total heat load for the nominal vehicle are moderate, an increase in the ballistic coefficient could cause them to be inordinately high. Finally, heating rates and total heat load for the higher velocities should be determined once models are developed for the higher entry speeds.

List of References

List of References

1) Konopliv, A. S., W.B. Banerdt, W.L. Sjogren, "Venus Gravity: 180th Degree and Order Model," Icarus, 1999, (in press).

2) Hunten, D. M., L. Colin, T. M. Donahue, and V. I. Moroz, Venus, The University of Arizona Press, 1983.

3) Muth, William D., "A Study of the Earth Return Aerocapture for Manned Mars Mission," Masters Thesis, The University of Tennessee, Knoxville, August 2000

4) Hoffmann, Cristoph S., "Aerocapture Studies for Future Mars Missions," Masters Thesis, The University of Tennessee, Knoxville, October 2000

5) Wercinski, P. F. and J. E. Lyne, "Mars Aerocapture: Extension and Refinement," *The AIAA Journal of Spacecraft and Rockets*, Vol. 31, No. 4, pp. 703-705, 1994.

6) Lyne, J. E., "Physiological Constraints on Deceleration During the Aercapture of Manned Vehicles," published as an abstract in *Aviation, Space, and Environmental Medicine*, May 1992 and complete paper published in *The AIAA Journal of Spacecraft and Rockets*, Vol. 31. No3, pp 443-446, 1994.

7) Lyne, J. E. and R. D. Braun, "Flexible Strategies for Manned Mars Missions Using Aerobraking and Nuclear Thermal Propulsion," *The Journal of the Astronautical Sciences*, Vol. 41, No. 3, pp. 339-348, 1993.

8) Lyne, J. E., "The Effect of Parking Orbit Selection on Manned Aercapture at Mars," *The AIAA journal of Spacecraft and Rockets*, Vol. 30, No. 4, pp. 484-487, 1993.

9) Lyne, J. E. , M. E. Tauber, and R. D. Braun, "Parametric Study of Manned Aerocapture: Part I: Earth Return from Mars", *The AIAA Journal of Spacecraft and Rockets*, Vol. 29, No. 6, pp. 808-813, 1992.

10) Lyne, J. E., A. Anagnost, and M. E. Tauber, "Parametric Study of Manned Aerocapture: Part II: Mars Entry," *The AIAA Journal of Spacecraft and Rockets,* Vol. 29, No. 6, pp. 814-819, 1992.

11) Braun, R. D., R. Powell, and J. E. Lyne, "Earth Aerobraking Strategies for Manned Return from Mars," *The AIAA Journal of Spacecraft and Rockets*, Vol. 29, No. 3, pp 297-304, 1992.

12) Graves, Claude A. and Jon C. Harpold, "Re-entry Targeting Philosophy and Flight Results from Apollo 10 and 11," AIAA paper number 70-28, AIAA 8th Aerospace Sciences Meeting, New York, January 19-21, 1970.

13) Bolling, Lamar, "Project Apollo: Apollo 6 Entry Postflight Analysis," MSC Internal Note No. 68-FM-299, Mission Planning and Analyisis Division, NASA, December 18, 1968.

14) Powell, R. W., S. A. Striepe, P. N. Desai, and R. D. Braun, "Program to Optimize Simulated Trajectories (POST) Utilization Manual," NASA Langley Research Center, Hampton, VA, September 1996.

15) Burgess, Eric, Venus: An Errant Twin, Columbia University Press, New York, 1985.

16) Jastrow, R., S. I. Rasool, The Venus Atmosphere, Institute of Space Studies, Goddard Space Flight Center, NASA, New York, New York, 1969.

17) NASA's IDS Webpage, 1998, http://vab02.larc.nasa.gov/IDS98.

18) Moore, Patrick, The Planet Venus, The Macmillan Company, New York, 1960.

19) Cattermole, Peter, Venus: The Geological Story, The John Hopkins University Press, Baltimore, Maryland, 1994.

20) Dunne, James A. and Eric Burgess, The Voyage of Mariner 10, Jet Propulsion Laboratory, California Institute of Technology, NASA, 1978.

21) Pioneer Venus Project Information, D.R. Williams, 2001, http://nssdc.gsfc.nasa.gov/planetary/pioneer_venus.html

22) Kneeland, A., A.S.Craig, C.Davis, E.Gorney, H.Holbrook, S.Huskins, R.Power, M.Sells, and Y.Suwa, "An Investigation of Crew Return Vehicle Configurations for a Manned Mars Mission," University of Tennessee, Knoxville Senior Design Project, 1998.

23) Spencer, David A., Robert C. Blandchard, Robert D. Braun, Pieter H. Kallemeyn, and Sam W. Thurman, "Mars Pathfinder Entry, Descent, and Landing Reconstruction," *Journal of Spacecraft and Rockets*, Vol. 36, No 3. pg. 357-366.

24) Page, W.A. and Woodward, H. T., "Radiative and Convective Heating During Venus Entry," *AIAA Journal*, Vol. 10, No. 10, Oct. 1972, pp. 1379-1381.

25) Private communication with Michael Tauber, formerly of NASA Ames Research Center and Stanford University.

26) Wiesel, W.E., Spaceflight Dynamics, Irwin/McGraw-Hill, 1997.

27) Rocket Science by Paul Woodmansee, 2000
http://www.woodmansee.com/science/rocket/r-other/rb-fuels.html

Appendix

Appendix

Input Decks

The following pages contain the post input decks used for the trajectory determination. Each deck is configured to calculated the minimum angle for the undershoot or the maximum angle for the overshoot. To clear any confusion, the sign convention used for gammai is set in POST as negative due to the nature of the trajectory. Each deck is specialized for a specific run, but can be altered fairly simply. To use these decks, one must first familiarize oneself with the workings of POST and understand for what each flag or variable stands. The comments are only listed for quick reference to what each parameter does. There are many values for every parameter, and again the POST manual must be consulted to determine which is correct for the run. These decks show how subtle changes can give vastly different results. All three are very similar, except for critical changes in either the density profile, aerodynamic coefficients, or target parameters.

The following table is used to calculate the overshoot trajectory for the nominal vehicle on the daytime side of Venus.

```
ccccccccccccccccccccccccccc
c   Venus Aerocapture       c
c    Overshoot optimization c
c Scott Craig               c
c                           c
ccccccccccccccccccccccccccc
l$search
    srchm=4,                            / Projected Gradient Targeting
    ioflag=3,                           / inputs & outputs in SI units
    ipro=1,
    maxitr=20,                          / Maximum number of Iterations
    irscl=3,
    isens=1,
c
c    Optimization Variable
c
    opt=-1,                              / minimize optimization
variable
    optvar='gammai',                    / Variable to optimize
    optph=1,                        / Phase at which to optimize variable
    wopt=-0.130,    / weight of the optimized variable
c
c Constraint Variables
c
    ndepv=1,        / number of constraints
c
    depvr(1)='malta',      / 1st constraint variable name
    depph(1)=100,          / phase at which to satisfy 1st constraint
    depval(1)=407.0,       / desired value of 1st constraint
    deptl(1)=10,         / tolerance () on 1st constraint
    idepvr(1)=0,           / upper bound constraint
c
c Control Variables
c
    nindv=1,         / number of controls
c
    indvr='gammai',        / names of controls
    indph=1,               / phases at which controls occur
    u=-11.1221976,              / initial guess for controls
    pert=1.0e-12,          / perturbation sizes for targeting routine
c
c
 $
l$gendat
    title=0h*Venus Aerocapture*,  / input deck title
    prnt(1)= 'time','veli','gdalt','asmg','gammai','dens','bnkang',

'banki','energy','cd','cl','period','malta','maltp','dynp',
```

```
            'xmax1','alpha','beta','dragw','pstop',
c
    event=1,                              / current event number
    fesn=100,                              / final event number
    npc(1)=3,                             / Keplerian conic calculation
    npc(2)=1,                             / Runge-Kutta integration
       dt=1.0,                                 / integration step size
    pinc=20.0,                            / print interval
    prnca=1,                            /ascii plotting interval
    prnc=1,                               / ploting interval (cannot be <
    monx(1)='asmg',                      /moniter max g-load
c
c state vector
c
    npc(4)=2,                             / position in spherical
       gdalt=180000.0,                        / altitude
       long=0.0,                               / longitude
       gclat=0.0,                              / geocentric latitude
    npc(3)=2,                             / velocity in planet-relative
       azveli=90.0,                            / inertial azimuth
       veli=1.40e4,                           / inertial velocity
    npc(12)=1,                            / calculate downrange,
crossrange
c
c atmospheric parameters
c
    npc(5)=1,                             / input atmosphere
    npc(8)=2,                             / aero coefficient option: input
    npc(6)=0,                             / no atmospheric winds
    npc(15)=1,                            / heat rate calc. flag
    npc(16)=0,                            / oblate planet
        j2=0.196972335776e-05,
        j3=-0.796824637191e-06,
        j4=-0.715808750045e-06,
        j5=0.140788849936e-06,
        j6=-0.323127644398e-07,
        j7=0.729578034332e-07,
        j8=0.425832531474e-06,
       mu=3.2502e,                  / gravitational parameter
       re=6051000.0,                        / equatorial radius
       rp=6051000.0,                        / polar radius
       omega=-2.9927e-07,          / Venus rotation rate (rad/s)
    wgtsg=2940,                      / force (N) = (mass*Earth g)
    sref=3.14159,                          / reference area (m2)
c
c GUIDANCE OPTION to define initial attitude
c
    iguid(1)= 0,             / use aerodynamic angles: alpha, beta, and
    iguid(2)= 0,             / same steering option for all aerodynamic
    iguid(3)= 1,             / cubic polynomial steering with constant
term
c                            / to alppc(1), betpc(1), and bnkpc(1)
       alppc(1)=0.0,              / initial alpha
       betpc(1)=0.0,              / initial beta
       bnkpc(1)=180.00,           / initial bank
```

```
 $
l$tblmlt   $
c
c Venus atmospheric data from reference
c
l$tab table=5hdenst,1,6haltito,71,1,1,1,
    0.0,6.50e01,  2000,5.87e01,  4000,5.29e01,
    6000,4.76e01,  8000,4.25e01,  10000,3.79e01,
    12000,3.38e01,  14000,2.98e01,  16000,2.63e01,
    18000,2.32e01,  20000,2.04e01,  22000,1.78e01,
    24000,1.55e01,  26000,1.35e01,  28000,1.17e01,
    30000,1.01e01,  32000,8.61,  34000, 7.34,
    36000,6.19,  38000,5.20,  40000,4.32,
    42000,3.56,  44000,2.91,  46000,2.37,
    48000,1.91,  50000,1.55,  52000,1.25,
    54000,9.99e-01,  56000,7.92e-01,  58000,6.08e-01,
    60000,4.51e-01,  62000,3.30e-01,  64000,2.36e-01,
    66000,1.68e-01,  68000,1.14e-01,  70000,7.89e-02,
    72000,5.45e-02,  74000,3.73e-02,  76000,2.54e-02,
    78000,1.71e-02,  80000,1.15e-02,  82000,7.65e-03,
    84000,5.00e-03,  86000,3.17e-03,  88000,1.95e-03,
    90000,1.17e-03,  92000,6.90e-04,  94000,4.02e-04,
    96000,2.31e-04,  98000,1.32e-04,  100000,7.64e-05,
    104000,2.66e-05,  108000,9.36e-06,  112000,3.36e-06,
    116000,1.23e-06,  120000,4.66e-07,  124000,1.82e-07,
    128000,7.30e-08,  132000,3.05e-08,  136000,1.33e-08,
    140000,6.01e-09,  144000,2.87e-09,  148000,1.43e-09,
    152000,7.54e-10,  156000,4.16e-10,  160000,2.35e-10,
    164000,1.44e-10,  168000,9.42e-11,  172000,6.43e-11,
    176000,4.48e-11,  180000,3.22e-11,
 $
c
c Cd table
c
l$tab table='cdt',0,1.224, $
c
c Cl table
c
l$tab table='clt',0,0.4321,
    endphs=1,
 $
c
c final event at exist: altitude = 407000 km
c
l$gendat
   event=100,critr='gdalt',value=407000.0,
   endphs=1,endprb=1,endjob=1,
 $
```

The following POST deck calculates the targeted periapse undershoot on the nocturnal side of Venus with the nominal vehicle.

```
ccccccccccccccccccccccccccc
c   Venus Aerocapture       c
c   Undershoot optimization c
c   A. Scott Craig          c
c                           c
ccccccccccccccccccccccccccc
1$search
    srchm=4,                            / Projected Gradient Targeting
    ioflag=3,                           / inputs & outputs in SI units
    ipro=1,
    maxitr=20,                          / Maximum number of Iterations
    irscl=3,
    isens=1,
c
c    Optimization Variable
c
    opt=-1,                              / minimize optimization
variable
    optvar='gammai',                    / Variable to optimize
    optph=1,                         / Phase at which to optimize variable
c    wopt=-0.130,    / weight of the optimized variable
c
c Constraint Variables
c
    ndepv=2,        / number of constraints
c
    depvr(1)='maltp',   / 1st constraint variable name (periapse)
    depph(1)=100, / phase to satisfy 1st constraint
    depval(1)=112,      / Desired value
    deptl(1)=10,  / tolerance
    idepvr(1)=1,  / Upper bound
c
    depvr(2)='malta',     / 2nd constraint variable name
    depph(2)=100,         / phase to satisfy 2nd constraint
    depval(2)=407.0,      / Desired value
    deptl(2)=15,          / tolerance
    idepvr(2)=0,          / equality constraint
c
c Control Variables
c
    nindv=2,         / number of controls
c
    indvr='gammai','critr',       / names of controls
    indph=1,50,              / phases at which controls occur
    u=-7.79,81.48511,  / initial guess for controls
    pert=1.0e-3,1.0e-3,   / perturbation sizes for targeting routine
c
c
 $
```

```
l$gendat
    title=0h*Venus Aerocapture*,  / input deck title
    prnt(1)= 'time','veli','gdalt','asmg','gammai','dens','bnkang',

'banki','energy','cd','cl','period','malta','maltp','dynp',
            'xmax1','alpha','beta','dragw','pstop',
c
    event=1,                          / current event number
    fesn=100,                          / final event number
    npc(1)=3,                         / Keplerian conic calculation
    npc(2)=1,                         / Runge-Kutta integration
       dt=1.0,                              / integration step size
    pinc=20.0,                          / print interval
    prnca=1,                         /ascii plotting interval
    prnc=1,                            / ploting interval (cannot be <
    monx(1)='asmg',                    /moniter max g-load
c
c state vector
c
    npc(4)=2,                          / position in spherical
       gdalt=180000.0,                     / altitude
       long=0.0,                            / longitude
       gclat=0.0,                           / geocentric latitude
    npc(3)=2,                         / velocity in planet-relative
c       gammai=-7.79,
       azveli=90.0,                         / inertial azimuth
       veli=1.20e4,                       / inertial velocity
    npc(12)=1,                        / calculate downrange,
crossrange
c
c atmospheric parameters
c
    npc(5)=1,                          / input atmosphere
    npc(8)=2,                          / aero coefficient option: input
    npc(6)=0,                          / no atmospheric winds
    npc(15)=1,                         / heat rate calc. flag
    npc(16)=1,                         / oblate planet
        j2=0.196972335776e-05,
        j3=-0.796824637191e-06,
        j4=-0.715808750045e-06,
        j5=0.140788849936e-06,
        j6=-0.323127644398e-07,
        j7=0.729578034332e-07,
        j8=0.425832531474e-06,
       mu=3.2502e+14,                 / gravitational parameter
       re=6051000.0,                      / equatorial radius
       rp=6051000.0,                      / polar radius
       omega=-2.9927e-07,       / Venus rotation rate (rad/s)
    wgtsg=2940,                     / force (N) = (mass*Venus g)
    sref=3.14159,                        / reference area (m2)
c
c GUIDANCE OPTION to define initial attitude
c
    iguid(1)= 0,          / use aerodynamic angles: alpha, beta, and
```

```
    iguid(2)= 0,          / same steering option for all aerodynamic
    iguid(3)= 0,          / cubic polynomial steering with constant
term
c                         / to alppc(1), betpc(1), and bnkpc(1)
       alppc(1)=0.0,           / initial alpha
       betpc(1)=0.0,           / initial beta
       bnkpc(1)=0.00,         / initial bank
 $
l$tblmlt   $
c
c Venus atmospheric data from reference
c
l$tab table=5hdenst,1,6haltito,71,1,1,1,
    0.0,6.50e01,  2000,5.87e01,  4000,5.29e01,
    6000,4.76e01,  8000,4.25e01,  10000,3.79e01,
    12000,3.38e01,  14000,2.98e01,  16000,2.63e01,
    18000,2.32e01,  20000,2.04e01,  22000,1.78e01,
    24000,1.55e01,  26000,1.35e01,  28000,1.17e01,
    30000,1.01e01,  32000,8.61,  34000, 7.34,
    36000,6.19,  38000,5.20,  40000,4.32,
    42000,3.56,  44000,2.91,  46000,2.37,
    48000,1.91,  50000,1.55,  52000,1.25,
    54000,9.99e-01,  56000,7.92e-01,  58000,6.08e-01,
    60000,4.51e-01,  62000,3.30e-01,  64000,2.36e-01,
    66000,1.68e-01,  68000,1.14e-01,  70000,7.89e-02,
    72000,5.45e-02,  74000,3.73e-02,  76000,2.54e-02,
    78000,1.71e-02,  80000,1.15e-02,  82000,7.65e-03,
    84000,5.00e-03,  86000,3.17e-03,  88000,1.95e-03,
    90000,1.17e-03,  92000,6.90e-04,  94000,4.02e-04,
    96000,2.31e-04,  98000,1.32e-04,  100000,7.40e-05,
    104000,2.75e-05,  108000,9.31e-06,  112000,2.93e-06,
    116000,8.56e-07,  120000,2.26e-07,  124000,4.99e-08,
    128000,1.22e-08,  132000,3.35e-09,  136000,1.02e-09,
    140000,3.26e-10,  144000,1.25e-10,  148000,5.41e-11,
    152000,2.63e-11,  156000,1.42e-11,  160000,7.91e-12,
    164000,4.57e-12,  168000,2.65e-12,  172000,1.55e-12,
    176000,9.33e-13,  180000,5.69e-13,
 $
l$tab table='denkt',0,1.0,  / density table multiplier
 $
c
c
c Cd table
c
l$tab table='cdt',0,1.224, $
c
c Cl table
c
l$tab table='clt',0,0.4321,
    endphs=1,
 $
l$gendat
    event=50,critr='tdurp',  / signal to start roll maneuver
    bnkpc(2)=10.0,
    endphs=1,
```

```
 $
l$gendat
    event=75,critr='bnkang',value=180.0,  /signal to end roll
    bnkpc(1)=180.0,                    / maneuver
    bnkpc(2)=0.0,
    endphs=1,
 $
c
c final event at exit: altitude = 407000 km
c
l$gendat
   event=100,critr='gdalt',value=407000.0,
   endphs=1,endprb=1,endjob=1,
 $
```

This final POST deck evaluates the undershoot with no roll maneuvers for the alternate angle of attack on the nocturnal side of Venus.

```
ccccccccccccccccccccccccccc
c   Venus Aerocapture       c
c   Undershoot optimization c
c Scott Craig               c
c                           c
ccccccccccccccccccccccccccc
l$search
    srchm=4,                            / Projected Gradient Targeting
    ioflag=3,                           / inputs & outputs in SI units
    ipro=1,
    maxitr=20,                          / Maximum number of Iterations
    irscl=3,
    isens=1,
c
c    Optimization Variable
c
    opt=1,                              / minimize optimization variable
    optvar='gammai',                    / Variable to optimize
    optph=1,                      / Phase at which to optimize variable
    wopt=-0.130,     / weight of the optimized variable
c
c Constraint Variables
c
    ndepv=1,         / number of constraints
c
    depvr(1)='malta',      / 1st constraint variable name
    depph(1)=100,          / phase at which to satisfy 1st constraint
    depval(1)=407.0,       / desired value of 1st constraint
    deptl(1)=10,         / tolerance () on 1st constraint
    idepvr(1)=0,           / upper bound constraint
c
c Control Variables
c
    nindv=1,          / number of controls
c
    indvr='gammai',        / names of controls
    indph=1,               / phases at which controls occur
    u=-7.676167961852,              / initial guess for controls
    pert=1.0e-12,           / perturbation sizes for targeting routine
c
c
 $
l$gendat
    title=0h*Venus Aerocapture*,  / input deck title
    prnt(1)= 'time','veli','gdalt','asmg','gammai','dens','bnkang',

'banki','energy','cd','cl','period','malta','maltp','dynp',
             'xmaxl','alpha','beta','dragw','pstop',
c
```

```
    event=1,                              / current event number
    fesn=100,                            / final event number
    npc(1)=3,                             / Keplerian conic calculation
    npc(2)=1,                             / Runge-Kutta integration
       dt=1.0,                                 / integration step size
    pinc=20.0,                           / print interval
    prnca=1,                          /ascii plotting interval
    prnc=1,                              / ploting interval (cannot be <
    monx(1)='asmg',                      /moniter max g-load
c
c state vector
c
    npc(4)=2,                             / position in spherical
       gdalt=180000.0,                       / altitude
       long=0.0,                              / longitude
       gclat=0.0,                             / geocentric latitude
    npc(3)=2,                             / velocity in planet-relative
       azveli=90.0,                           / inertial azimuth
       veli=1.40e4,                          / inertial velocity
    npc(12)=1,                            / calculate downrange,
crossrange
c
c atmospheric parameters
c
    npc(5)=1,                             / input atmosphere
    npc(8)=2,                             / aero coefficient option: input
    npc(6)=0,                             / no atmospheric winds
    npc(15)=1,                            / heat rate calc. flag
    npc(16)=0,                            / oblate planet
        j2=0.196972335776e-05,
        j3=-0.796824637191e-06,
        j4=-0.715808750045e-06,
        j5=0.140788849936e-06,
        j6=-0.323127644398e-07,
        j7=0.729578034332e-07,
        j8=0.425832531474e-06,
       mu=3.2502e+14,                    / gravitational parameter
       re=6051000.0,                          / equatorial radius
       rp=6051000.0,                          / polar radius
       omega=-2.9927e-07,           / Venus rotation rate (rad/s)
    wgtsg=2940,                        / force (N) = (mass*Earth g)
    sref=3.1416,                           / reference area (m2)
c
c GUIDANCE OPTION to define initial attitude
c
    iguid(1)= 0,              / use aerodynamic angles: alpha, beta, and
    iguid(2)= 0,              / same steering option for all aerodynamic
    iguid(3)= 1,              / cubic polynomial steering with constant
term
c                             / to alppc(1), betpc(1), and bnkpc(1)
       alppc(1)=0.0,               / initial alpha
       betpc(1)=0.0,               / initial beta
       bnkpc(1)=0.00,             / initial bank
 $
l$tblmlt   $
```

```
c
c Venus atmospheric data from reference
c
l$tab table=5hdenst,1,6haltito,71,1,1,1,
    0.0,6.50e01,  2000,5.87e01,  4000,5.29e01,
    6000,4.76e01,  8000,4.25e01,  10000,3.79e01,
    12000,3.38e01,  14000,2.98e01,  16000,2.63e01,
    18000,2.32e01,  20000,2.04e01,  22000,1.78e01,
    24000,1.55e01,  26000,1.35e01,  28000,1.17e01,
    30000,1.01e01,  32000,8.61,  34000, 7.34,
    36000,6.19,  38000,5.20,  40000,4.32,
    42000,3.56,  44000,2.91,  46000,2.37,
    48000,1.91,  50000,1.55,  52000,1.25,
    54000,9.99e-01,  56000,7.92e-01,  58000,6.08e-01,
    60000,4.51e-01,  62000,3.30e-01,  64000,2.36e-01,
    66000,1.68e-01,  68000,1.14e-01,  70000,7.89e-02,
    72000,5.45e-02,  74000,3.73e-02,  76000,2.54e-02,
    78000,1.71e-02,  80000,1.15e-02,  82000,7.65e-03,
    84000,5.00e-03,  86000,3.17e-03,  88000,1.95e-03,
    90000,1.17e-03,  92000,6.90e-04,  94000,4.02e-04,
    96000,2.31e-04,  98000,1.32e-04,  100000,7.40e-05,
    104000,2.75e-05,  108000,9.31e-06,  112000,2.93e-06,
    116000,8.56e-07,  120000,2.26e-07,  124000,4.99e-08,
    128000,1.22e-08,  132000,3.35e-09,  136000,1.02e-09,
    140000,3.26e-10,  144000,1.25e-10,  148000,5.41e-11,
    152000,2.63e-11,  156000,1.42e-11,  160000,7.91e-12,
    164000,4.57e-12,  168000,2.65e-12,  172000,1.55e-12,
    176000,9.33e-13,  180000,5.69e-13,
 $
c
c Cd table
c
l$tab table='cdt',0,1.28, $
c
c Cl table
c
l$tab table='clt',0,0.257,
    endphs=1,
 $
c
c final event at exist: altitude = 407000 km
c
l$gendat
   event=100,critr='gdalt',value=407000.0,
   endphs=1,endprb=1,endjob=1,
 $
```

Vita

Anthony Scott Craig was born on January 14th, 1975 in Memphis, Tennessee. After living in the city for a couple of years, his family moved to the suburb of Bartlett. He attended elementary school and high school in Bartlett receiving good grades throughout and finally graduating from Bolton High School in the top 5 percent of a class of nearly 300. Outside of school he was very active in church and boy scouts, helping his church start its own scout troop and achieving the rank of Eagle Scout in December of 1992. Also active in high school band, he was section leader for the baritone section his junior and senior year in high school. Showing an aptitude towards science and math, he decided to pursue engineering as an occupation. With a scholarship to Christian Brothers University, he attended the first two years of his college career there, majoring in Mechanical Engineering. After a great deal of thought, he decided to change majors and transfer to the University of Tennessee, Knoxville to work on Aerospace Engineering. Graduating with a Bachelor of Science in Aerospace Engineering in December of 1998, he then decided to continue his education to obtain a Masters of Science in Aerospace Engineering which he will receive in August of 2002 following the acceptance of this thesis.